Lithos 332–333 (2019) 245–260

Contents lists available at ScienceDirect

Lithos

journal homepage: www.elsevier.com/locate/lithos

Petrology of alkaline silicate rocks and carbonatites of the Chuktukon massif, Chadobets upland, Russia: Sources, evolution and relation to the Triassic Siberian LIP

Anna G. Doroshkevich [a,b,c,*], Dmitry A. Chebotarev [a], Victor V. Sharygin [a,d,e], Ilya R. Prokopyev [a,d], Anna M. Nikolenko [a]

[a] V.S. Sobolev Institute of Geology and Mineralogy SB RAS, prosp.Akad. Koptyuga, 3, Novosibirsk 630090, Russia
[b] Geological Institute SB RAS, Sakhyanovoy Str., 6a, Ulan-Ude 670047, Russia
[c] Tomsk State University, Lenin Ave., 36, Tomsk 634050, Russia
[d] Novosibirsk State University, Pirogova Str., 2, Novosibirsk 630090, Russia
[e] Institute of Physics and Technology, Ural Federal University, Mira Str., 2, Ekaterinburg 620002, Russia

ARTICLE INFO

Article history:
Received 17 September 2018
Accepted 5 March 2019
Available online 08 March 2019

Keywords:
Melilitites
Damtjernites
Carbonatites
Chadobets upland
Triassic Siberian LIP
Source characteristics

ABSTRACT

The petrogenesis of temporally and spatially associated carbonatitic and deeply derived carbonated alkaline silicate magmas provides an opportunity to gain insights into the nature of the deepest lithospheric mantle. The Chuktukon massif, which is part of the Chadobets alkaline ultramafic carbonatite complex (Chadobets upland, Siberian craton) is a carbonatite-melilitite-damtjernite intrusion, whose emplacement was coeval with the Siberian Traps large igneous province (LIP). In this study, the sources of the primary melts are examined, the petrogenetic evolution of the complex is reconstructed and the relationship with the Siberian LIP is also discussed. Isotopic and geochemical information indicate that the source for the Chuktukon primary melts was isotopically moderately depleted and the primary melts were formed by low degree partial melting of garnet carbonated peridotite. Hydrothermal processes caused ^{18}O- and ^{13}C- enrichment. The weathering process was accompanied by trace element re-distribution and enrichment of the weathering crust in Zn, Th, U, Nb, Pb and REE, relative to the Chuktukon rocks and a change in radiogenic (Sr, Nd) isotope compositions.

1. Introduction

The Chadobets alkaline ultramafic carbonatite complex is located within the Chadobets upland (basin of the Chadobets River, Krasnoyarsk Territory, Russia) at the southern part of the Siberian craton (Fig. 1). The Chadobets upland is 40 × 50 km in size and is elongated in a NNW direction. It is surrounded by a system of ring faults and includes the Chuktukon and Terina ledges (also known as Chuktukon and Terina massifs). The uplift is related to the ascent of a magmatic diapir and the formation of an intermediate magma chamber at a depth of 4 km that is confirmed by geophysical data (Kirichenko et al., 2012). The Chadobets upland occurs at the intersection of two Neoproterozoic graben basins that are part of Angara-Kotuy large-scale rift system (Fig. 2a) (Dashkevich, 1999; Staroseltsev, 2009). The Chadobets complex comprises ultramafic-alkaline silicate rocks (melilitites, damtjernites) and carbonatites. The carbonatites and their weathering crust host major reserves of Nb (39.8 Mt. at 0.6 wt% of Nb_2O_5) and REE (486 Mt. at 7.3 wt% of REE_2O_3) (Lomayev and Serdyuk, 2011).

Chebotarev et al. (2017a) reported a U—Pb (SHRIMP II) age of 252 ± 12 Ma for perovskite from the melilitites and an Ar—Ar age of 231 ± 2.7 Ma for the rippite (new mineral $K_2(Nb,Ti)_2(Si_4O_{12})O(O,F)$ discovered in the the carbonatite of the Chuktukon massif (Doroshkevich et al., 2016)). The emplacement of the rocks was coeval with volcanic-magmatic activity such as the Siberian flood basalts (e.g., Burgess and Bowring, 2015), carbonatites and alkaline ultramafic rocks of the Maymecha–Kotuy province (e.g. Basu et al., 1995; Dalrymple et al., 1995; Ghobadi et al., 2018; Kogarko and Zartman, 2011; Malich et al., 2015), as well as the Siberian kimberlites and lamproites (Carlson et al., 2006; Ernst et al., 2018; Ivanov et al., 2013; Letnikova et al., 2014; Sun et al., 2014; Vasyukova, 2017; Vrublevskii et al., 2005). The relationship between Siberian flood basalts and alkaline rocks, however, is still poorly studied. For example, numerous previous studies provided different interpretations of the sources for the Siberian flood basalts: partial melting of the lithospheric mantle; direct derivation from a mantle plume; a MORB-like source; or the interaction of plume-derived magmas with the continental crust (e.g. Fedorenko et al., 1996; Lightfoot et al., 1993; Sharma et al., 1991, 1992; Wooden et al., 1993).

* Corresponding author at: V.S. Sobolev Institute of Geology and Mineralogy SB RAS, prosp.Akad. Koptyuga, 3, Novosibirsk 630090, Russia.
E-mail address: doroshkevich@igm.nsc.ru (A.G. Doroshkevich).

https://doi.org/10.1016/j.lithos.2019.03.006
0024-4937/

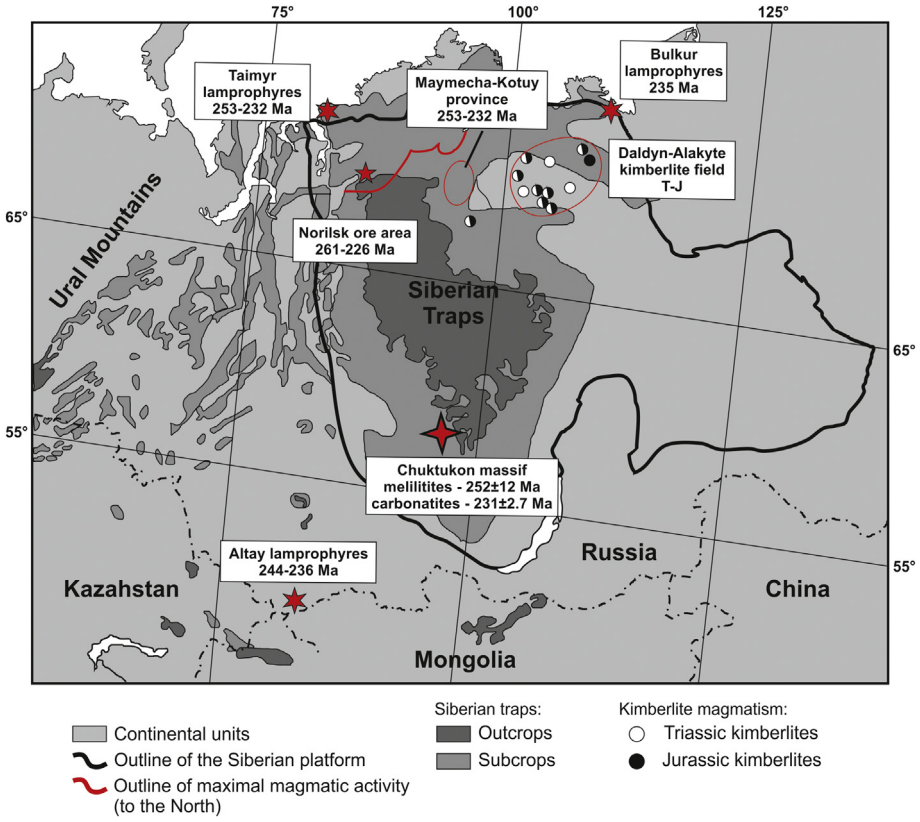

Fig. 1. Location of the Late Permian–Triassic basalts related to the Siberian Superplume and contemporaneous alkaline complexes. The area of high activity of the Siberian basalt magmatism is located above a thick red line (Sobolev et al., 2011). Ages are taken from Basu et al. (1995), Dalrymple et al. (1995) Kogarko and Zartman (2011), Malich et al. (2015), Ghobadi et al. (2018), Vrublevskii et al. (2005); Carlson et al. (2006), Sun et al. (2014), Vasyukova (2017), Ivanov et al. (2013), Letnikova et al. (2014), Zaitsev and Smelov (2010), Chebotarev et al. (2017a).

In contrasts, contributions concerning the geochemical and isotopic studies of the alkaline rocks are limited (e.g., Arndt et al., 1998; Fedorenko et al., 2000; Vrublevsky et al., 2005; Carlson et al., 2006; Kogarko and Zartman, 2011; Ghobadi et al., 2018; Ivanov et al., 2018). The existing data indicate that Siberian flood basalts and alkaline rocks may be related to different sources and/or melting conditions.

Nevertheless, the study of temporally and spatially associated carbonatitic and deeply derived carbonated silicate magmas (e.g., ultramafic lamprophyres) is very important because their origin has been generally attributed to partial melting of carbonated peridotite of the deepest lithospheric mantle (Agashev et al., 2008; Dalton and Presnall, 1998; Downes et al., 2005; Gudfinnsson and Presnall, 2005; Tappe et al., 2017; Walter et al., 2008), and provides an opportunity to gain insight into the relationship and evolution of carbonate-rich mantle-derived melts.

In this study, we present petrographic, and the first geochemical and isotopic data for the alkaline ultramafic rocks and carbonatite samples as well as their weathering crust collected from drill cores of the Chuktukon massif to understand the sources, petrogenesis and evolution of the complex as well as their relationship with the Siberian LIP.

2. Geological background

As discussed earlier, the Chadobets upland is located in at the intersection of several rift grabens (Fig. 2) that are characterized by Devonian and Triassic ultramafic-alkaline magmatism. The Devonian Ilbokich complex is located approximately 70 km to the southwest of the Chadobets uplift (Fig. 2). Ilbokich ultramafic lamprophyres (of aillikite and damtjernite composition) form a dyke swarm with individual dykes ranging from few centimeters up to 4 m. Their detailed petrography, mineralogy and geochemistry have been presented in previous studies (Kargin et al., 2016; Nosova et al., 2018). The Triassic Chadobets complex includes alkaline ultramafic rocks and carbonatites of the Chuktukon and Terina massifs (Fig. 2). The alkaline ultramafic rocks are predominant at the Terina massif, whereas the carbonatites are dominant at the Chuktukon massif. The petrographic and mineralogical characteristics of ultramafic-alkaline magmatism of the Chadobets upland (Chuktukon and Terina massifs) have been reported in a number of publications (e.g., Kirichenko et al., 2012; Lapin, 1997, 2001; Lapin and Lisitzyn, 2004; Slukin, 1994; Tsikyna, 2004).

The country rocks for the Chadobets complex are Neoproterozoic and Cambrian sedimentary detrital and carbonate rocks such as metamorphic rocks, sandstones, limestones, dolostones, and siltstones (Fig. 2). The periphery of the upland is composed of Permian-Carboniferous and Lower Triassic sedimentary rocks (sandstones, siltstones, argillites, dolostones, conglomerates, coal, gravels, tuffs) and areas of subhorizontal Lower Triassic traps. Igneous rocks within the Chadobets upland are not exposed at the surface, but are overlain by Cretaceous-Cenozoic alluvial sediments (clays with sand interlayers). The complex comprises the following sequence of rocks from the earliest to the latest: alkaline ultramafic rocks (alkaline picrite, olivine melilitite and others), carbonatites and then damtjernites (Kirichenko et al., 2012; Lapin, 1997, 2001; Lapin and Lisitzyn, 2004; Slukin, 1994). Alkaline ultramafic rocks form a dyke swarm and sills ranging in thickness from a few centimeters up to 120 m. Carbonatites are present as small stocks (up to 2.5 × 1.5 km), dykes and sills (up to 20 m thick and over 2–3 km long). The contacts of carbonatites with country rocks are sharp and marked by banded textures, which are caused by a preferred orientation of the main minerals within the carbonatites. The carbonatites and ultramafic rocks are typically surrounded by thin

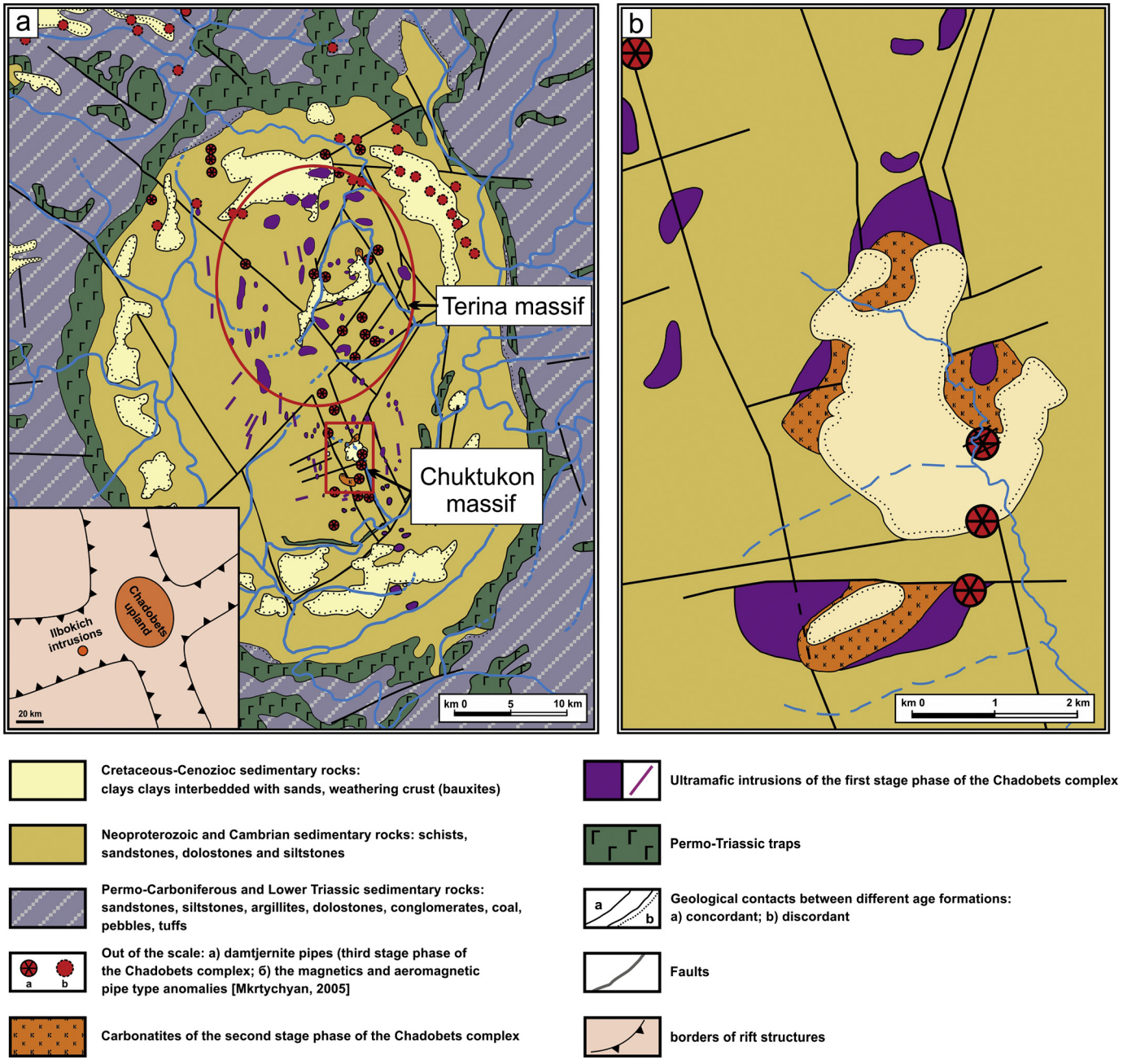

Fig. 2. a - Geological scheme of the Chadobets upland after Kirichenko et al. (2012). Data for inset are taken from Dashkevich (1999). b – Geological scheme of the Chuktukon massif (unpublished data from geological report of "Krasnoyarskgeols'emka", 2010).

potassic feldspar-aegerine or apatite-phlogopite fenite zones (up to 10–20 cm wide) within the country rocks. Damtjernites pipes and diatremes (several tens, from 30 × 120 to 700 × 600 m in size) occur in a central part of the upland (in a longitudinal zone). Damtjernites cut ultramafic rocks and carbonatites and often contain their xenoliths. In general, all igneous rocks of the complex are intensely altered by hydrothermal and weathering processes. Weathering crust is developed upon the diverse rocks of the massif, and varies from 5 to 40 m in thickness, sometimes reaching up to 480 m (Kirichenko et al., 2012). The general structure of the weathering crust includes the disintegration zone (lower part of the weathering profile) and the ochre zone (the upper part of the profile) (Slukin, 1994; Tsikyna, 2004). The border between zones of weathering crust is very variable and not well defined. Monazite from weathered crust overlying carbonatites yielded a U—Pb (SHRIMP II) date of 102.6 ± 2.9 Ma (Chebotarev et al., 2017a).

3. Analytical methods

Minerals were examined using an optical petrographic microscope Olympus BX51 and by energy dispersive spectrometry in combination with a scanning electron microscope using a TESCAN MIRA 3 LMU JSM-6510LV equipped with INCA Energy 450 XMax 80 microanalysis system (Oxford Instruments Ltd.). The chemical compositions of the minerals were analyzed using a JEOL JXA-8100 electron microprobe. For silicates and carbonates, a beam current of 10 nA and an acceleration voltage of 15 kV were used while for Fe—Ti oxides these parameters were 20 nA and 15 kV. Data were calibrated using natural minerals and synthetic phases. In order to colour potassic feldspar in yellow, some thin sections of damtjernites were etched in fumes of hydrofluoric acid for 2–3 min and covered by a water solution (10 ml) of cobalt nitrate (2 g) in acetic acid (1 ml) and washed in running water after 15 min.

Prior to powdering of damtjernite samples, all fragments containing visible xenolithic material were removed by hand picking. Whole-rock compositions were determined by X-ray fluorescence (ARL-9900-XP). Trace and REE element analyses by ICP-MS were performed using a Finnigan MAT under standard operating conditions (open acid digestion using a HF, HNO_3 and $HClO_4$ mixture). The detection limits were determined using 3σ criteria of the blank and ranged from 0.005 up to 0.1 μg/g for a majority of elements. The investigations were carried out at the Analytical Center for Multi-Elemental and Isotope Research Siberian Branch, Russian Academy of Science (Novosibirsk, Russia).

The Nd and Sr isotopic compositions were measured using a Finnigan MAT 262 multicollector mass spectrometer using Re and Ta filaments operated in static mode at the Geological Institute of Kola Scientific Centre RAS, Apatity, Russia. The reproducibility of the Rb, Sr, Sm, and Nd determinations was estimated to be ±0.5% from the replicate analyses of the BCR standard. The total blanks were 0.05 ng for Rb, 0.2 ng for Sr, 0.06 ng for Sm, and 0.3 ng for Nd. Data were evaluated measurements of the La Jolla and SRM-987 standards. The Sr isotope composition was normalized to $^{87}Sr/^{86}Sr = 8.37521$, and the Nd composition was normalized to $^{146}Nd/^{144}Nd = 0.7219$. The Nd isotope composition was corrected to $^{143}Nd/^{144}Nd = 0.511860$ in the La Jolla standard. εNd and $T_{DM}(Nd)$ were calculated using the CHUR value (Bouvier et al., 2008) and the DM value (Goldstein and Jacobsen, 1988), accordingly.

$\delta^{18}O_{SMOW}$ and $\delta^{13}C_{PDB}$ values were analyzed in carbonates using a Finnigan MAT 253 sensitive mass spectrometer at the Geological Institute SB RAS (Ulan-Ude, Russia). The CO_2 was extracted from minerals at 60 °C during 2–4 h reaction with H_3PO_4. The international reference materials NBS-18 and NBS-19 were used to assess the accuracy of results. The analytical errors for the $\delta^{18}O$ and $\delta^{13}C$ values were ± 0.05‰ and ± 0.1‰, respectively.

4. Petrography and mineralogy

4.1. Melilitite

Classifying of ultramafic rocks from the Chuktukon massif is problematic because the rocks are altered by hydrothermal processes. Nevertheless, the rocks were identified as olivine melilitite based on the petrography of fresh alkaline ultramafic rocks from the coeval and proximal Terina massif (e.g., Kirichenko et al., 2012; Lapin, 1997, 2001; Lapin and Lisitzyn, 2004; Slukin, 1994). According to the latter studies, melilitites of the Terina massif are massive porphyritic rocks with olivine phenocrysts (up to 30%). The groundmass is composed of olivine (up to 20%), clinopyroxene (up to 10%), phlogopite (up to 15%), melilite (ákermanite, up to 10%), and carbonates (up to 10%). Minor and accessory minerals are nepheline, apatite, perovskite, garnet (andradite), spinel-group minerals, and zircon.

The Chuktukon rocks are massive porphyritic rocks and composed primarily of completely altered olivine (?) phenocrysts in a fine-grained groundmass (Fig. 3). Alteration products of the phenocrysts are calcite and serpentine-group minerals. Perovskite, dolomite, phlogopite-kinoshitalite, fluorapatite, spinel-group minerals and garnet (andradite-grossular) are common in the groundmass. Monazite-(Ce), zircon, Zr- and Nb-bearing rutile (up to 1.2 wt% of ZrO and up to 1.6 wt% of Nb_2O_5), calzirtite, sulphides, and titanite are accessory minerals. The secondary groundmass minerals are calcite, chlorite-, cancrinite- and kaolinite-groups minerals, barite, quartz, and romanéchite. Most probably, cancrinite- and kaolinite-groups minerals replace aluminosilicate minerals (nepheline, melilite) during hydrothermal alteration (due to migration of CO_2-rich acid fluids).

The spinel-group minerals occur as composite crystals rather than single-phase grains. Typically, Cr-spinel cores are mantled by tiny Ti-magnetite or magnetite rims (Fig. 3). The composition of the minerals generally follow a "titanomagnetite trend" for spinel in orangeites and ultramafic lamprophyres (Mitchell, 1995; Tappe et al., 2005) with increasing Fe, Ti and decreasing Mg, Al and Cr (Table 1, Fig. 4). The $Fe_t^{2+}/(Fe_t^{2+}+Mg)$ ratio varies from 0.4 to 1. Cr# is up to 0.65.

Mica displays strong concentric zonation (Fig. 3) reflecting variations in the phlogopite-kinoshitalite modal proportions, with a Ba-poor core and a Ba-rich rim. The mineral contains low amounts of TiO_2 (up to 1.8 wt%) and MnO (up to 0.9 wt%), has negligible amounts of F (below detection limit), and is enriched in MgO (up to 22 wt%) (see Supplementary material). Variations in Si, Al, K and Ba indicate that the major exchange-reaction is Ba + Al ↔ K + Si. Examples of structural formula are indicated below:

$$(K_{0.82}Ba_{0.10})_{0.92}\ (Mg_{2.51}\ Fe_{0.47}\ Mn_{0.04}Ti_{0.09})_{3.11}\ (Si_{2.86}\ Al_{1.14})_{4.00}\ O_{20}\ [OH_{1.91}O_{0.09}]_{2.00}$$

$$(Ba_{0.66}\ K_{0.30})_{0.96}\ (Mg_{2.19}\ Fe_{0.39}\ Mn_{0.02}\ Al_{0.30}\ Ti_{0.06})_{2.96}\ (Si_{2.02}\ Al_{1.98})_{4.00}\ O_{20}\ [OH]_{4.00}$$

Such Ba-rich micas are typical of many kimberlites (Mitchell, 1995) and rocks of alkaline carbonatite complexes, for example, in the olivinites of the Guli massif from the Maymecha–Kotuy province in Russia (Kogarko et al., 2012), and in the metasomatized mantle xenoliths (Kogarko et al., 2007).

4.2. Damtjernites

The Chuktukon ultramafic lamprophyres are classified as damtjernite based on the mineralogical composition and the classification scheme established by Tappe et al. (2005). The damtjernites have brecciated textures (Fig. 3) with clasts of country rocks, alkaline ultramafic rocks, carbonatite and mantle xenoliths (peridotites, eclogites) (Kirichenko et al., 2012; Lapin, 2001). Macrocrysts (up to 30% of rock volume) consist of phlogopite, dolomite-ankerite and pseudomorphs of a rhombic mineral, probably of the olivine group, replaced by quartz-dolomite aggregates (Fig. 3). The macrocrysts occur in an interstitial fine-grained matrix of carbonates (dolomite-ankerite and calcite) (up to 40%), potash feldspar (up to 7%), phlogopite-tetraferriphlogopite (up to 10%) and spinel-group minerals (up to 5–7%). Minor and accessory minerals are fluorapatite, sulphides, ilmenite, rutile (up to 3 wt% Nb_2O_5 and up to 2 wt% ZrO_2) and, fluorcalciopyrochlore. Secondary minerals are quartz, strontianite, daqingshanite-(Ce) and barite. The rocks are abundant in pelletal lapilli in which the cores of the macrocrysts are surrounded by dolomite-potassic feldspar microlithic material with K-feldspar and dolomite plates, and calcite, rutile, spinel, apatite and phlogopite micrograins (Fig. 3).

Cr-spinel occurs as small discrete euhedral crystals (fractions of mm) and exhibits an atoll texture surrounded by thin rings of Ti-magnetite (Fig. 3). Mineral compositions (see Supplementary material) are in good agreement with the published compositional "titanomagnetite trend" of spinels (Mitchell, 1995; Tappe et al., 2005) (Fig. 4) and minerals have Cr# is as high as 0.60. The spinel compositions are consistent with those of ultramafic lamprophyre (Tappe et al., 2005).

Primary dolomite-ankerite from the groundmass (see Fig. 3, k), lapilli and macrocrysts is Sr-bearing (Table 3), and has variable composition ranging from dolomite to Mg-rich ankerite (see Supplementary material). Late carbonate replacing olivine (?) is Fe-rich dolomite and has lower SrO content (see Supplementary material).

Macrocrysts of phlogopite are enriched in TiO_2 and Cr_2O_3 (see Supplementary material). In contrast, the groundmass micas are enriched in F and depleted in TiO_2 and Cr_2O_3 (see Supplementary material). Mica compositions are consistent with the Al-enrichment trends for orangeites and ultramafic lamprophyres (Mitchell, 1995; Tappe et al., 2005) (Fig. 5).

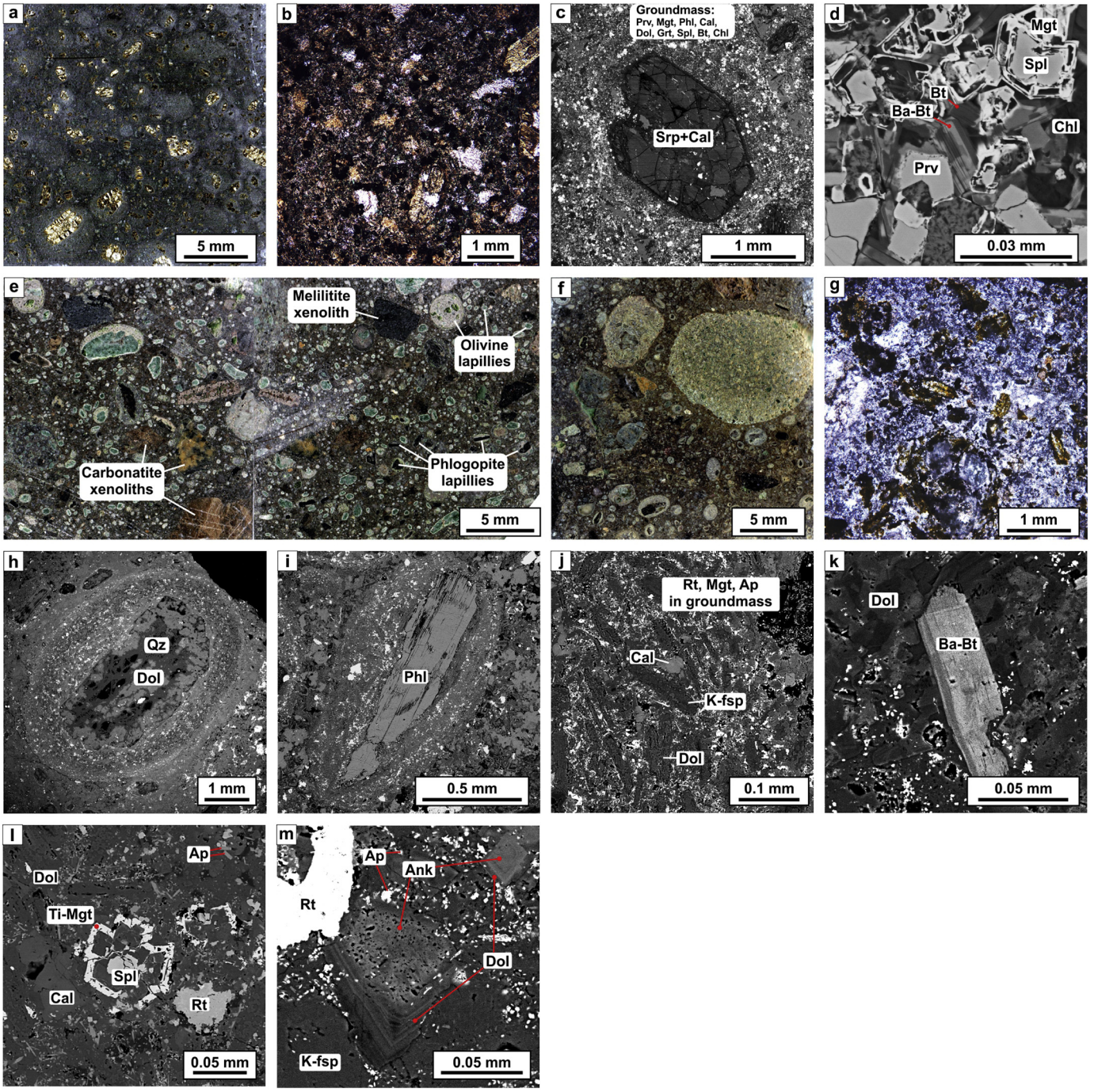

Fig. 3. Photomicrographs (a, b, e-g) and BSE images (c-d, h-m) of mineral textures of the Chuktukon alkaline silicate rocks: a-d – melilitites; e-m – damtjernites; a – porphyritic texture of melilitites, b – melilitite groundmass; c – olivine (replaced by aggregate of serpentine (Srp) and calcite) crystal in melilitite groundmass, composed by perovskite (Prv), magnetite (Mgt), phlogopite (Phl), calcite (Cal), dolomite (Dol), garnet (Grt), spinel (Spl), biotite (Bt), chlorite (Chl); d – melilitite groundmass with crystals of Cr-spinel mantled by magnetite rims and zoned Ba-rich biotite (Ba-Bt) grains; e-f - porphyritic-brecciated texture of damtjernites; g - texture of damtjernite groundmass. Potash feldspar (K-fsp) has been colored in yellow after etching (see Section 3 for description); h-i - lapilli with olivine (replacing by quartz-dolomite) and phlogopite (phl) cores, respectively; j – structure of lapilli: laths of potash feldspar and dolomite; k – zoned biotite in damtjernite groundmass; l –atoll structure of Cr-spinel in Ti-mgt ring in damtjernite; m – ankerite(Ank) -dolomite in damtjernite groundmass. Abbreviations are from Whitney and Evans (2010).

4.3. Carbonatites

Doroshkevich et al. (2016), Sharygin et al. (2016a, 2016b), Sharygin (2017), Sharygin and Doroshkevich (2017), and Chebotarev et al. (2017b) carried out detailed studies of the petrography and mineralogy of the carbonatites.

The carbonatites are fine- and medium-grained rocks with massive, spotty and banded textures (Fig. 6). The primary mineral assemblage includes calcite, fluorcalciopyrochlore, rippite, tainiolite, fluorapatite, fluorite, Nb-rich rutile (up to 17 wt% of Nb_2O_5), K-feldspar, aegirine, dolomite, ancylite-Ce, strontianite, olekminskite, sulphides, and zircon. Calcite is speckled with dolomite spots and fine disseminations of ancylite-(Ce), strontianite, and olekminskite. The SrO concentration in calcite is up to 0.8 wt% (see Supplementary material). The chemical compositions of rippite and tainiolite are close to the ideal structural formula for these minerals, $K_2(Nb,Ti)_2(Si_4O_{12})O(O,F)$ and $KMg_2Li(Si_4O_{10})F_2$, respectively (Doroshkevich et al., 2016; Sharygin, 2017; Sharygin et al., 2016a).

Table 1
Major (wt%) and trace element (ppm) composition of the Chuktukon rocks.

Rock	Weakly altered carbonatite				Strongly altered carbonatite					Weathering crust (disintegrated zone and ochres)						Damtjernite		Melilitite					Terina*
Sample	549,197	539150c	539150t	546,193	549,149	549,190	539,137	539,202	539,132	539,083	538,132	516108a	546108b	543,028	514,066	546,046	546,054	514,231	514,236	535,067	514,239	514,218	
	1	2	3	4	5	6	7	8	9	10	11	12	13	14	15	16	17	18	19	20	21	22	23
wt%																							
SiO_2	1.41	1.81	0.56	3.34	18.20	14.59	23.70	17.03	65.05	47.50	80.30	1.74	2.62	4.30	2.62	14.60	16.02	19.95	23.78	18.08	18.04	26.54	23.90–29.39
TiO_2	0.10	0.07	0.02	0.07	0.03	0.33	0.10	0.09	0.09	0.07	0.08	1.12	0.89	1.00	0.22	2.34	2.57	3.01	3.02	3.56	3.11	3.34	2.52–4.48
Al_2O_3	0.19	0.14	0.41	0.14	0.21	0.13	0.17	0.16	1.85	0.26	0.23	3.84	3.80	6.83	2.51	3.83	3.38	4.91	4.99	5.05	5.58	5.79	3.42–5.67
FeO	2.93	3.71	1.63	4.92	3.33	4.37	5.59	5.04	5.05	4.13	7.23	67.77	64.38	74.23	60.49	9.81	9.39	11.26	10.74	11.26	10.57	13.88	11.30
MnO	0.78	0.59	0.49	0.32	0.37	1.01	1.65	1.10	1.14	2.69	4.63	0.57	2.82	0.75	3.90	0.53	0.70	0.42	0.18	0.11	0.56	0.59	0.21–0.34
MgO	0.39	2.84	0.38	0.11	0.48	0.11	0.31	0.26	0.27	0.13	0.18	0.38	0.13	0.09	0.11	11.31	8.31	10.25	12.98	7.81	8.39	18.11	12.59–13.88
CaO	51.65	47.59	53.39	48.8	42.44	42.56	37.01	40.47	13.19	23.70	1.15	0.61	0.71	0.40	0.36	22.29	24.67	25.41	21.53	27.11	25.10	14.39	15.27–20.50
Na_2O	0.05	0.14	0.13	0.05	0.15	0.12	0.14	0.10	0.18	0.20	0.10	0.25	0.28	0.12	0.10	0.32	0.29	0.09	0.11	0.06	0.23	0.09	0.52–1.20
K_2O	0.08	0.02	0.02	0.12	0.08	0.03	0.03	0.03	0.79	0.04	0.04	0.04	0.07	0.05	0.09	2.50	2.47	0.28	0.62	0.89	3.98	0.68	1.78–2.52
P_2O_5	0.66	0.30	0.41	0.66	0.70	0.05	0.30	3.24	0.96	15.92	1.15	3.56	3.68	2.29	0.28	0.92	0.90	1.34	1.54	1.11	1.80	1.63	0.91–1.62
BaO	0.44	0.74	0.59	0.91	0.09	0.47	0.63	0.78	0.36	0.49	1.07	0.61	0.96	0.42	0.06	0.28	0.21	0.18	0.38	0.10	0.25	0.68	
SO_3	0.22	8.15	6.07	2.46	4.55	0.18	0.27	0.33	4.03	0.11	0.10	0.01	0.04	0.02	0.03	0.77	0.29	0.08	0.21	0.08	0.09	5.22	
LOI	40.97	33.60	35.92	37.37	28.40	34.51	29.36	29.11	5.58	1.48	1.91	11.43	11.25	5.50	29.22	29.46	29.92	22.20	19.41	24.03	22.07	7.60	
Total	99.88	99.58	99.90	99.28	98.93	98.39	99.14	97.75	98.56	96.72	98.17	92.20	91.85	96.22	100.02	99.11	99.26	99.56	99.69	99.43	99.78	98.75	
ppm																							
V	235	65	51	71	118	142	147	190	172	117	226	1570	1301	1180	55	197	218	163	252	203	250	291	140–290
Cr	8.6	3.5	3.5	8.0	8.1	11.6	35.4	12.0	21.8	20.9	14.6	31.5	29.3	36.4	11.7	526.7	385.3	636.2	671.9	676.7	705.5	654.3	390–550
Co	1.9	1.3	0.5	2.1	19.4	4.7	31.8	6.2	4.8	6.1	3.2	6.6	27.3	3.4	6.0	48.3	28.1	55.6	43.0	42.0	57.9	30.2	33–145
Ni	3.1	3.0	3.0	2.8	5.1	3.0	10.4	6.5	7.3	21.3	9.8	6.1	12.9	5.7	3.0	257.0	156.5	256.0	339.0	304.2	291.6	180.3	48–365
Cu	24.4	6.8	27.5	25.4	22.4	23.9	30.4	16.5	35.5	185.3	31.7	36.6	32.8	24.4	13.4	59.5	46.5	40.6	68.9	59.2	74.8	82.7	50–360
Zn	272	54	36	40	312	221	231	266	279	1839	987	4308	4567	6827	841	447	461	88	129	449	271	720	210–940
Rb	3.3	1.5	0.6	0.5	0.8	1.6	0.5	1.3	16.5	1.2	1.7	0.6	0.6	1.1	3.8	91.8	48.4	17.3	30.1	41.7	31.1	221.8	
Sr	1820	2004	2176	19,526	6166	1649	1111	1785	669	711	1123	5968	5469	1984	124	1271	1653	1521	2272	897	2467	1077	1200–1500
Y	113.6	71.6	81.0	98	120.4	146	80.9	252.5	61.3	127.3	366	1383	1231	1257	53.2	86.6	103	26	34.8	38.3	57.4	57.5	23–37
Zr	59.6	9.8	8.8	88.3	94.9	172.6	12	36.9	21.9	30.5	75.5	399.8	348.3	391.2	62.7	205.2	270.2	288.2	284.3	419	347.5	286.7	210–460
Nb	1338	44.5	16.5	602.5	626	2673	67.2	1759	88	213	284.8	14,000	14,700	4805	86	386.4	636.5	165	308	187.3	267.8	579.7	180–790
Mo	2.8	0.9	2.2	1.9	6.2	4.3	10.5	9	9.9	66.8	24.2	32.6	17.9	48.4	6.2	1.4	8.3	1.6	3.3	2.7	0.9	4.0	3–19
Ba	3755	5652	4482	4896	792	3815	5619	6394	2758	3988	9292	4731	7817	3278	340	2297	1872	1374	3263	844	5659	2064	800–3280
La	556.6	670.4	817	825.6	921	695.4	740	673.6	1394	1596	4089	6616	7309	4850	781	375	515	149.3	182.7	137	769.2	244.4	160–240
Ce	955.4	1181	1465.3	1499	1790	1384	1234	1279	2589	1344	6349	10,195	12,372	5720	847.3	655.4	817.3	307.2	320	194	1055	436.3	200–300
Pr	103.3	134.4	166.2	171	208.8	163.4	130	151	230	265.2	589.2	1135.5	1187	683.4	81	73.3	86.6	33.9	36.3	27.2	97.8	45.3	
Nd	369.4	459.2	553.8	570.8	799.7	596.5	440.3	567	574	834.2	1749	3870	3907	2139	228.3	262.7	296.4	130	134.6	96	300	159.5	
Sm	55	54.5	63.7	67.7	125.7	87	57.6	91	43	108.5	211	562.8	532.7	284.6	26.7	41	44	19.8	20.7	16.3	38.9	25.2	
Eu	14.6	13	15.8	17.2	34.6	24.7	15.4	25.6	10.3	28.2	54.2	158.8	144.8	76.2	6.6	11	12.1	5.3	5.5	4.4	9.7	6.6	
Gd	44.2	37.6	43.7	45.9	91.7	72.9	44.9	73.5	36.1	77.4	164.9	458.6	423.2	245.7	20	31.9	36.6	14.6	16.7	12.2	29.5	20.2	
Tb	5.5	4.1	4.5	5.5	10	9	4.9	10	3.5	8.3	18.8	53	46.9	28.9	2.5	3.9	4.4	1.8	1.9	1.6	3.3	2.5	
Dy	24.9	18.6	20.5	22.5	37.7	40.8	20.2	49.9	15.9	34.3	83.7	233	204.3	149.3	12.6	18.2	20.3	8.2	8	7.3	14.7	12	
Ho	4.1	3.1	3.3	4.5	5.2	6.5	3.3	8.6	2.6	5.4	14.1	42.8	37.3	31.3	2.2	3.2	3.6	1.3	1.3	1.3	2.4	2.2	
Er	9.6	7.9	9	11	11	15.1	7.3	22	6.7	12.8	36.2	114.4	102	89.3	6.5	7.8	8.5	2.7	3.3	3.7	5.8	5.8	
Tm	1.2	1.0	1.2	1.6	1.1	1.8	0.8	2.8	0.8	1.5	4.4	15.4	13.3	12.3	1.0	1.0	1.2	0.3	0.4	0.5	0.7	0.8	
Yb	5.5	6.2	6.8	7.0	4.7	9.1	4.5	14.2	4.5	7.1	21.2	87.8	74.5	67.6	6.3	5.8	6.1	1.8	2.2	3.0	3.8	4.8	
Lu	0.6	0.8	0.9	1.0	0.6	1.2	0.5	1.4	0.6	0.8	2.2	12.4	9.9	8.8	0.9	0.7	0.8	0.2	0.3	0.4	0.5	0.6	
Hf	0.5	0.2	0.2	0.3	1.7	0.7	0.4	0.5	0.6	1.1	1.9	6.6	5.1	6.7	1.7	6.1	10.5	6.9	6.4	8.9	7.5	7.0	
Ta	0.2	0.1	0.1	0.1	0.4	0.2	0.1	0.2	0.2	0.3	0.1	3.3	2.4	2.1	0.5	3.3	2.7	4.9	4.2	4.5	4.8	5.1	
Pb	16.3	11.6	10.8	11.2	8.9	30.7	32	13.7	23.4	47.3	208.6	259.4	235.3	255	40.8	35.3	23	12.9	12.1	6.9	37.1	65.7	5–51
Th	6.6	9.7	12.9	11.8	10.8	7.7	14.7	49.6	7.2	51.0	14.6	220	204.8	113.5	39	38	28	18.3	17.8	14.3	26	17.4	
U	5.0	0.9	0.9	0.9	0.6	9.3	1.7	0.9	3.8	0.8	16.4	25.5	23.7	14.6	0.6	0.9	0.9	4.8	3.6	2.6	5.7	2.5	
Ce/Pb	59	102	135	134	201	45	39	93	111	28	30	39	53	22	21	19	35	24	26	28	28	7	
Nb/U	266	48	19	669	1103	287	40	1959	23	256	17	549	619	330	145	434	713	34	85	71	47	228	

Note: Variations of the major and trace elements in alkaline ultramafic rocks from the coeval neighbored Terina massif (Lapin, 2001; Lapin and Pyatenko, 1992).

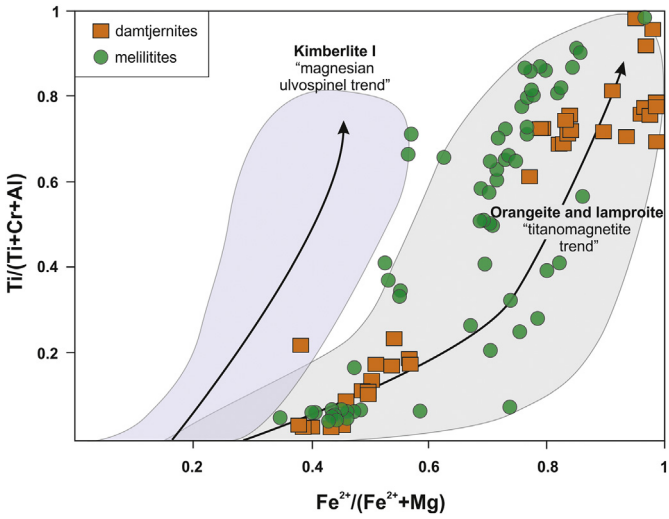

Fig. 4. Atomic Ti/(Ti + Cr + Al) vs $Fe^{2+}/(Fe^{2+}+Mg)$ plot for the spinel-group minerals in the Chuktukon melilitite and damtjernite. Kimberlite and orangeite trends are from Mitchell, 1995.

Barite, quartz, goethite, Sr-rich carbonate-fluorapatite (up to 7 wt% SrO), Ca-REE-fluorcarbonates (parisite-(Ce), synchysite-(Ce)), monazite-(Ce), Sr-Ba-Pb-rich hydropyrochlores and psilomelane (romanèchite ± hollandite aggregate) are related to a stage of metasomatic (hydrothermal) alteration of the carbonatites. These minerals occur interstitially among grains of primary minerals and/or form networks of microveinlets. Primary calcite is depleted in SrO (below detection limit) in hydrothermally altered parts of carbonatites. Goethite from hydrothermally altered carbonatites contains up to 2.2 wt% of Nb_2O_5 (Chebotarev et al., 2017b). Burbankite, strontianite, daqingshanite-(Ce), ferrohagendorfite, barite, burbankite-khanneshite, nyerereite (?), unidentified Na-REE-Ba-Sr-Ca-rich and Na-Fe-rich phosphates, and Na-rich hydrated carbonate occasionally appear in secondary multiphase inclusions in fluorapatite, zircon and calcite (Sharygin et al., 2016b; Sharygin and Doroshkevich, 2017). Primary zircon-hosted melt inclusions are carbonate-rich in composition and multiphase: calcite + dolomite or alkali-rich carbonates (nyerereite? + shortite + burbankite) (Sharygin and Doroshkevich, 2017).

4.4. Weathering crust

Slukin (1994), Tsikyna (2004) and Chebotarev et al. (2017b) presented detailed studies of the petrography and mineralogy of the weathering crust. Below, we provide a short description.

The weathering crust is composed of residual minerals (pyrochlore, rutile, and zircon) and minerals formed during weathering. The rocks are fine-grained, banded, and patchy-striped, which is expressed as alternating bands and spots of goethite and rare earth minerals (Fig. 6, b, c, e, f). The groundmass is composed of an aggregate of goethite andkaolinite (Fig. 6). Florencite-(Ce), monazite-(Ce), psilomelane (romanèchite ± hollandite aggregate), churchite-(Y), and daqingshanite-(Ce) are minor and accessory minerals. Usually, goethite forms complete pseudomorphs after fragments (up to 1 cm) of unidentified minerals. Florencite-(Ce) and monazite-(Ce) occur as irregularly shaped grains, up to 0.3 cm in size, as well as aggregates of micron-sized grains of intricately shaped patches, as well as network of vein-like segregations. Typically, both minerals have a porous internal structure. Churchite-(Y) forms radially fibrous 2–5 mm aggregates and individual 2–3 mm crystals. A network of psilomelane (romanèchite ± hollandite aggregate) microveinlets dissect the rocks.

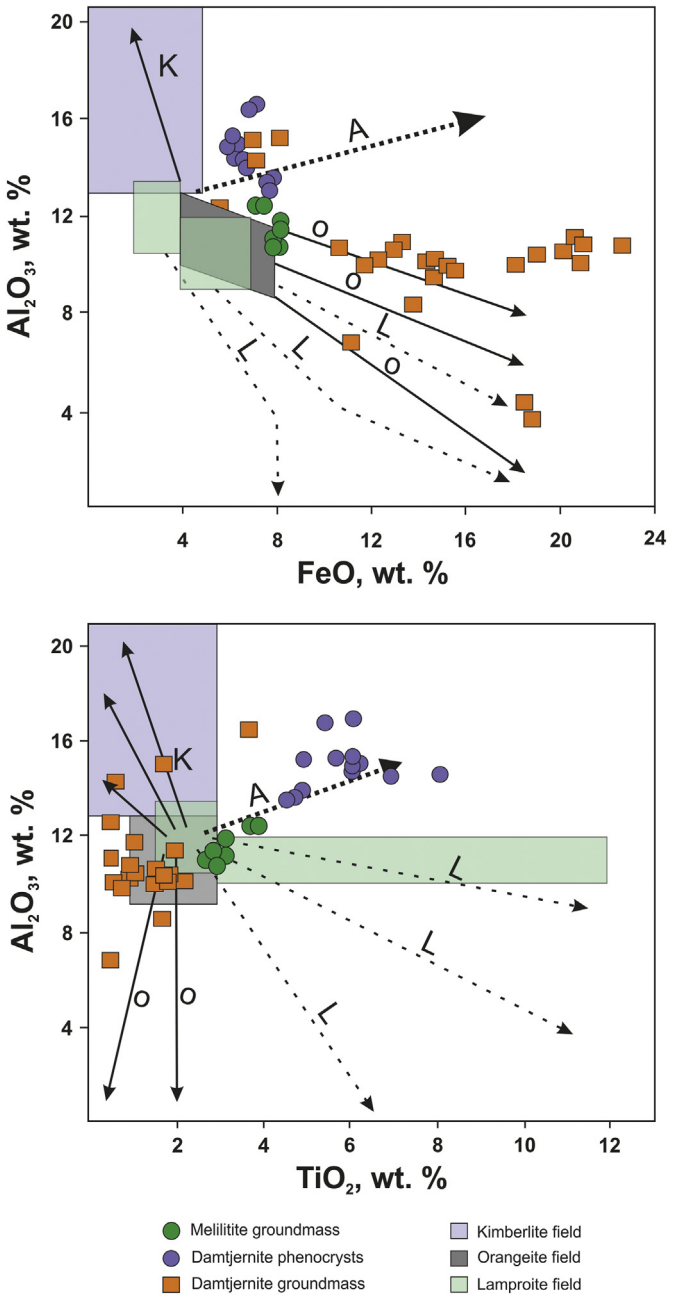

Fig. 5. Compositional trends of micas from the Chuktukon damtjernites and melilitites. K – kimberlite trends, O – orangeite trends, L – lamprophyre trends, A – aillikite trends (after Mitchell, 1995).

5. Whole-rock compositions

The results of major and trace element analyses of melilitite, damtjernites, carbonatites and weathering crust are presented in Table 1.

5.1. Melilitites and damtjernites

The melilitites and damtjernites are strongly silica undersaturated (up to 26 wt% SiO_2). These rocks are enriched in CaO (up to 28 wt%) and TiO_2 (up to 3.6 wt%), while MgO is variable (8.5–18 wt%). Damtjernites contain more K_2O than melilitites and its content is dependent on the abundance of phlogopite. Melilitites have normative larnite >10%. Both rock types have high Mg# number, 60 to 70. The major element contents of melilitites and damtjernites are in the same

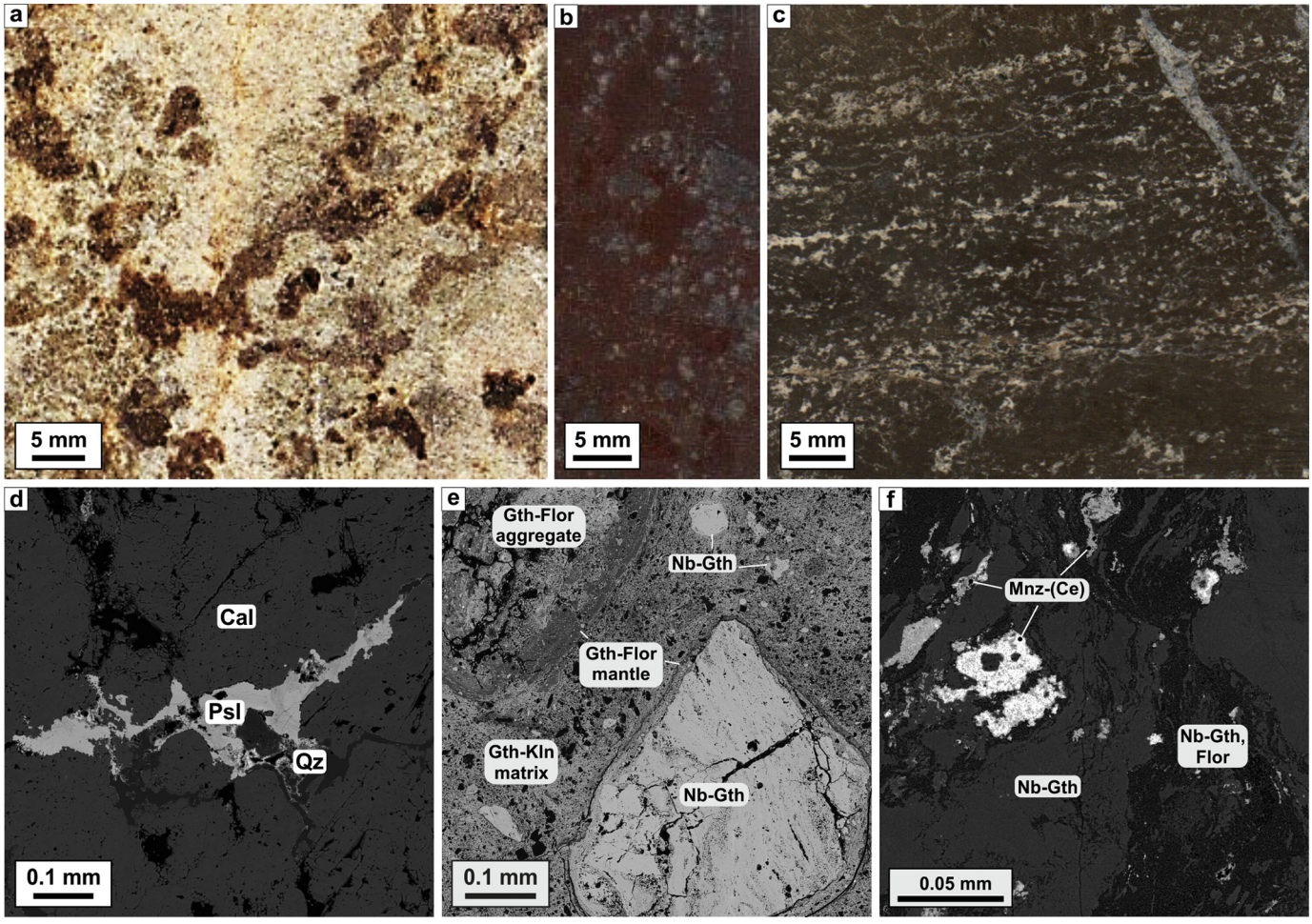

Fig. 6. Photomicrographs (a-c) and BSE images (d-f) of mineral textures of the Chuktukon carbonatites (a, d) and weathering crust (b, c, e, f).

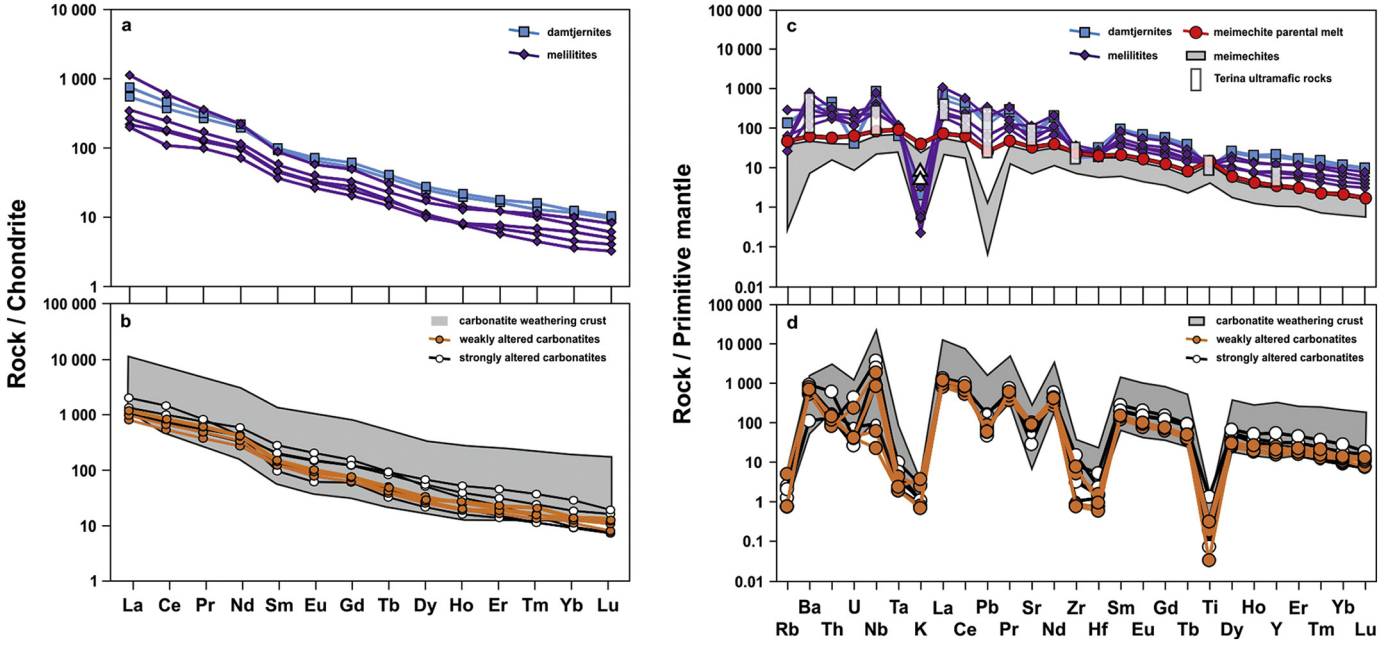

Fig. 7. Primitive mantle- and chondrite-normalized plots for the Chuktukon rocks. Normalizing values for primary mantle and chondrite are from Sun and McDonough (1989). Meimechites of Maymecha-Kotuy province are from Vasilyev et al. (2017), the calculated meimechite parental melt is from Sobolev et al. (2009), ultramafic rocks from the Terina massif are from Lapin and Pyatenko (1992), Lapin (2001).

Table 2
Sr—Nd isotopic composition of the Chuktukon rocks.

Rock	Sample	Sm (ppm)	Nd (ppm)	$^{147}Sm/^{144}Nd$	$^{143}Nd/^{144}Nd$	±2SD	εNd (0)	εNd (T)	T (DM)	Rb (ppm)	Sr (ppm)	$^{87}Rb/^{86}Sr$	$^{87}Sr/^{86}Sr$	±2SD	I (Sr)
Damtjernite	546054	45.6	300.4	0.091833	0.512693	7	1.08	4.43	574	39.1	1588	0.07118	0.70374	2	0.703487
	546046	41.0	262.8	0.094383	0.512693	7	1.08	4.34	586	92.3	1235	0.21612	0.70411	4	0.703341
Melilitite	514218	24.9	158.5	0.094948	0.512697	10	1.15	4.40	584	238.4	1041	0.66252	0.70475	4	0.702394
	514239	38.5	297.3	0.078344	0.512693	6	1.08	4.86	517	33.3	2419	0.03978	0.70363	4	0.703489
	514236	22.0	128.3	0.096552	0.512744	9	2.07	5.27	531	30.2	2284	0.03830	0.70373	3	0.703594
Strongly altered carbonatite	539202	90.3	566.1	0.096392	0.512738	18	1.95	5.16	538	1.3	1826	0.00213	0.70317	6	0.703162
	539137	58.4	439.4	0.080305	0.512677	13	0.76	4.48	543	0.5	1078	0.00127	0.70329	7	0.703285
Weakly altered carbonatite	539150t	64.6	530.7	0.073571	0.512686	12	0.94	4.87	507	0.4	2193	0.00058	0.70339	3	0.703388
	539150c	61.4	456.0	0.081404	0.512665	9	0.53	4.21	561	1.2	1993	0.00179	0.70326	4	0.703254
	549197	56.1	374.5	0.090592	0.512679	6	0.80	4.19	585	3.7	1795	0.00603	0.70303	4	0.703009
Weathering crust	539083	108.1	812.2	0.080474	0.512658	10	0.39	2.17	565	1.1	707	0.00441	0.70388	5	0.703872
	516108b	576.9	4003.8	0.087086	0.512672	7	0.67	2.35	578	0.3	5518	0.00017	0.70368	2	0.70368
	514066	27.7	228.3	0.073292	0.512605	12	−0.64	1.25	594	5.4	116	0.13482	0.70739	8	0.70716

range as those of fresh alkaline ultramafic rocks from the coeval and proximal Terina massif (Table 1). Fig. 7 shows chondrite-normalized rare earth element (REE) patterns for damtjernite and melilitite. All samples are strongly LREE enriched with La_{cn}/Yb_{cn} between 33 and 144. The damtjernite samples are more enriched in total REEs, but retain REE patterns that are sub-parallel to melilitites. The incompatible trace element abundances for damtjernite and melilitite are similar and show a significant enrichment in most elements, particularly in Nb and REEs, and pronounced troughs for Rb, Ta, K, Pb, Zr, and Hf (Fig. 7). Nb and Ta are hosted by perovskite (melilitite) and pyrochlore (damtjernite), while Zr and Hf mostly reside in zircon, perovskite and pyrochlore. Both rock types have Ni and Cr concentrations that are typical for mantle-derived primitive magmas (up to 350 ppm Ni; up to 700 ppm Cr). Ce/Pb and Nb/U ratios are variable, but remain high (6–35 and 34–434, respectively) (Table 1). Chuktukon patterns match well with the trace element levels from the fresh alkaline ultramafic rocks from the coeval Terina massif (Table 1, Fig. 7).

5.2. Carbonatites

This group of rocks consists of calciocarbonatites. Weakly hydrothermally altered carbonatites are characterized by low SiO_2 (up to 3.3 wt%), and MgO (up to 3 wt%) contents. The strongly hydrothermally altered carbonatites have higher SiO_2 (up to 65 wt%) than the less hydrothermally altered counterparts. Alkali content ($Na_2O + K_2O$) is low.

Chondrite-normalized REE profiles are similar for the weakly and strongly hydrothermally altered carbonatites with strong LREE enrichment (Fig. 7) and La_{cn}/Yb_{cn} is between 34 and 220. REEs in carbonatites mostly reside in apatite, monazite-(Ce), Ca-REE-fluorcarbonates (parisite-(Ce), synchysite-(Ce)), ancylite-(Ce), and pyrochlore.

As illustrated by the mantle-normalized trace element plots (Fig. 7), carbonatites are strongly enriched in Sr, Ba, Th, U, Nb and other elements. The rocks have variable Nb and Zr contents due to the irregular distribution of Nb- and Zr- minerals. The bulk Ba content depends on the amounts of barite and secondary romanéchite, and to a lesser degree, on the content of pyrochlore and K-feldspar in the rock. U, Nb and Ta mainly reside in pyrochlore, rippite, and secondary goethite (Chebotarev et al., 2017b) and Rb mainly reside in tainiolite and K-feldspar. Apart from pyrochlore, much of the Zr and Hf have accumulated in zircon. Compared to melilitites and damtjernites, the carbonatites have lower concentrations of Rb, Ta, K, Zr, Hf, Ti, Cr and Ni, and higher REE and Y content.

5.3. Weathering crust

The weathering crust has high concentrations of P (up to 15 wt%), reflecting its high contents of florencite-(Ce) and monazite-(Ce); the Al content is also high and is dependent of on the abundances of the kaolinite-group minerals, and to a lesser degree, of those of florencite-(Ce). Mn and Ba are hosted by romanéchite.

The weathering crust has variable but usually higher whole-rock REE content than the carbonatites, melilitites and damtjernites (Fig. 7) with a pronounced depletion in HREE relative to LREE (La/Yb_{CN} of up to 160). The REE budget in the weathering crust is dominated by florencite-(Ce) and monazite-(Ce) and, to a lesser degree, churchite-(Y) and pyrochlore.

The weathered rocks are enriched in Zn, Th, U, Nb, Pb and REE when compared with their corresponding fresh counterparts. Nevertheless, the configurations of the weathering crust mantle-normalized trace-element patterns are similar to those of the carbonatites, melilitites and damtjernites. Goethite and pyrochlore are the main hosts of Nb in the weathering crust, while Zn mostly resides in goethite (Chebotarev et al., 2017b).

6. Radiogenic (Sr, Nd) and stable (C, O) isotopic data

The results of radiogenic (Sr, Nd) isotopic analyses of melilitite, damtjernites and carbonatites, and the weathering crust are presented in Table 2. The initial Sr ratios and εNd of the alkaline rocks and the weathering crust were calculated assuming ages of 250 and 120 Ma, respectively (Chebotarev et al., 2017a). The alkaline silicate rocks and carbonatites have relatively heterogeneous Nd and Sr isotope compositions, ranging from +4.19 to +5.27, while $^{87}Sr/^{86}Sr$ (I) values vary from 0.7024 to 0.7036. In contrast, the initial $^{87}Sr/^{86}Sr$ ratios of the weathering crust are variable, and the εNd values are lower than those of the alkaline silicate rocks and carbonatites; this can be attributed to isotopic exchange of Nd and Sr with surrounding rocks during the weathering process. Fig. 8 shows a plot of the $^{87}Sr/^{86}Sr$(I) and εNd (T) for the Chuktukon rocks. It also includes initial Nd and Sr isotope compositions for the ultramafic and alkaline rocks of the Guli massif (Kogarko and Zartman, 2011), the Siberian meimechites and flood basalts (Sharma et al., 1991, 1992; Wooden et al., 1993; Lighfood et al., 1993; Arndt et al., 1998; Fedorenko et al., 2000; Carlson et al., 2006), and the Triassic Siberian kimberlites and lamproites (Carlson et al., 2006; Sun et al., 2014; Vasyukova, 2017; Vrublevskii et al., 2005). In the $^{87}Sr/^{86}Sr$ (I) vs. εNd (T) plot, the Chuktukon and Guli samples as well as meimechites and kimberlites fall within the Nd-enriched and Sr-depleted quadrant. High-Ti Siberian basalts display large Sr and Nd isotopic variations, partially overlapping the field of alkaline rocks and intersecting with the field of low-Ti Siberian basalts. Lamproite samples plot well within the low-Ti basalt field.

The $\delta^{18}O_{SMOW}$ and $\delta^{13}C_{PDB}$ values of carbonates from all rock types of the Chuktukon massif and country limestones are listed in Table 3 and plotted in Fig. 9. One value of carbonate from melteigite falls within the primary carbonatite box (Taylor Jr and Sheppard, 1986). The remaining carbonates have higher $\delta^{18}O_{SMOW}$. Of note, the variation in carbon isotope values is more limited in range, compared to the variation in

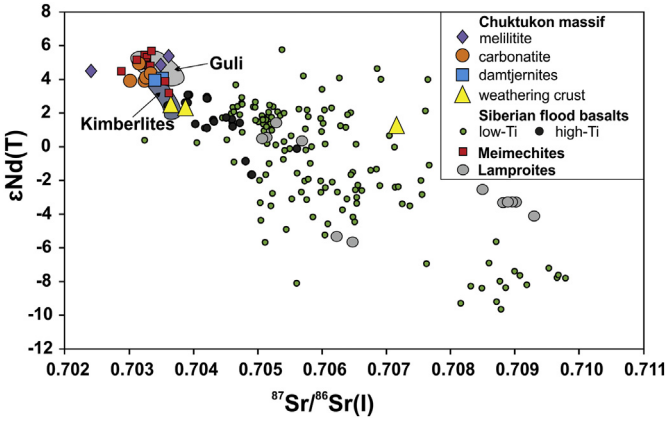

Fig. 8. $^{87}Sr/^{86}Sr(I)$vs εNd(T) plot for the Chuktukon rocks. Also shown are data for the ultramafic and alkaline rocks of the Guli massif (Kogarko and Zartman, 2011), the Siberian meimechites and flood basalts (Sharma et al., 1991, 1992; Wooden et al., 1993; Lighfood et al., 1993; Arndt et al., 1998; Fedorenko et al., 2000; Carlson et al., 2006; Ivanov et al., 2018), the Triassic Siberian kimberlites and lamproites (Carlson et al., 2006; Sun et al., 2014; Vasyukova, 2017; Vrublevskii et al., 2005).

corresponding oxygen isotope values (Table 3, Fig. 9). The $\delta^{18}O$ and $\delta^{13}C$ values for minerals from the Terina and Ilbokich ultramafic lamprophyres are very close to those of the Chuktukon rocks (Fig. 9). Such shifts of isotope values could be attributed to late-stage hydrothermal alteration and/or limestone assimilation (e.g., Deines, 1989; Demény et al., 2004; Santos and Clayton, 1995 and references therein). The isotopic variation of carbonates from the Chuktukon rocks can be related to hydrothermal alteration. This is in agreement with petrographic observations.

7. Discussion

7.1. Source characteristics of the Chuktukon magmas and evolution

The high Mg# number and the high Ni and Cr contents of the Chuktukon ultramafic alkaline rocks suggest that these crystallized from near primary peridotite mantle-derived melts and have not undergone significant fractional crystallization. In addition, melilitites, damtjernites and carbonatites show overlapping Sr and Nd isotopic compositions (see Fig. 8). This suggests that all magma types were derived from a common moderately depleted mantle source beneath the Siberian craton. The trace element enrichment of the Chuktukon rocks can be achieved by a very low degree of melting of their mantle source. Kogarko and Zartman (2011) and Ghobadi et al. (2018) proposed that high concentrations of trace elements in the Guli rocks was related to mantle metasomatism, which did not modify the initial isotopic signature of the depleted mantle source. The trace element data (high Sr and Nb, and La/Sm ratio) of the Chuktukon rocks suggest that the metasomatic agent is not a silicate fluid or melt but most likely the result of carbonatite metasomatism (Downes et al., 2002). Similarly, the presence of primary carbonate minerals in the Chuktukon alkaline silicate rocks as well as carbonatites indicates that the parental melt was enriched in carbonate. The trace element composition of the Chadobetz olivine (Nosova et al., 2018) and the presence of Ba-rich mica in the Chuktukon melilitites confirms that the primary melts were derived from a carbonate-rich source. In addition, strong light REE enrichment and heavy REE and Y depletion of the Chuktukon rocks may indicate that they were formed by a low degree of melting of a garnet-bearing source. This is consistent with the experimental data that indicate the generation of alkaline magmas by a low degree partial melting of carbonated garnet peridotite (e.g., Dalton and Presnall, 1998; Gudfinnsson and Presnall, 2005).

The lack of evidence for crustal contamination in the Chuktukon rocks is indicated by pronounced depletions in Pb, Zr—Hf, and HREE relative to similarly incompatible elements in the trace element patterns (see Fig. 7) as well as high Ce/Pb and Nb/U ratios compared to those of continental crust (Rudnick and Gao, 2003). This inference is supported by (1) the geochemical and Sr—Nd isotopic similarity with alkaline rock of the Maimecha-Kotuy province that appear to exclude crustal contamination (e.g. Basu et al., 1995; Ivanov et al., 2018; Kogarko and Zartman, 2011); and (2) the distinction from the Triassic Siberian lamproites (see Fig. 8) that appear to have a source contaminated by crustal materials (Vasyukova, 2017; Vrublevskii et al., 2005). The generation of primary melts for ultramafic lamprophyre-carbonatite series is usually attributed to partial melting of carbonated peridotite at >150 km depths (e.g. Agashev et al., 2008; Dalton and Presnall, 1998; Downes et al., 2005). Unfortunately, it is difficult to estimate the PT-parameters of the Chuktukon rock formation, using the olivine and olivine-spinel pair, considering that olivine is deeply altered, but it is possible to draw out an analogy with the Terina unaltered olivine. Nosova et al. (2018) determined the olivine equilibration temperature and pressure based on the composition of Terina alkaline ultramafic rocks; the estimated values are 1200 °C and 40–60 kbars. This is consistent with observations of Dashkevich (1999), who reported a 150–180 km depth of asthenosphere-lithosphere boundary beneath the Chadobets uplift. In addition, the calculated temperatures and pressures from the Terina olivines (Nosova et al., 2018) agree well with the Siberian pre-trap and post-trap mantle paleogeotherms (Howarth et al., 2014).

The oxygen fugacity (fO_2) for the Chuktukon alkaline ultramafic rocks was calculated using the equation of Ballhaus et al. (1991) with a temperature at 1100–1200 °C and pressure 4–6 GPa (according to Nosova et al., 2018) and the compositions of olivines and Cr-spinels from Chuktukon and Terina ultramafic lamprophyres (our data and Nosova et al., 2018). The calculated fO_2 ranges from FMQ +1.1 to +2.1 log units; the values are consistent with those obtained for meimechites of the Maymaecha-Kotuy province (Ryabchikov et al., 2009).

An important question raised by this study concerns the mechanism of the carbonatite formation at the Chuktukon. Two possibilities can be considered: (1) primary origin by partial melting of a carbonated mantle source; (2) silicate-carbonate liquid immiscibility.

Melting experiments of carbonated peridotite at pressures 3–10 GPa produce carbonatite melt by a low degree of partial melting; the melts have a magnesiocarbonatite composition rather than calciocarbonatite (e.g., Dalton and Presnall, 1998; Dasgupta et al., 2009; Foley et al., 2009; Klemme et al., 1995; Sweeney et al., 1995). The key features of direct mantle derived carbonatites were included in a summary table by Bell and Rukhlov (2004). They are dolomitic, have few, if any, associated silicate rocks and high Mg# values. They always contain some mantle minerals (Cr-rich minerals, diamond and/or graphite). Examples of direct mantle-derived carbonatites occur worldwide (e.g., Tamazert (Mourtada et al., 1997); Shawa and Dorowa (Harmer and Gittins, 1998), Newania (Doroshkevich et al., 2010); Spitskop (Harmer, 1999);

Table 3
Isotopic composition of O and C in carbonates from the Chuktukon rocks.

Rock type	Sample	Mineral	$\delta^{18}O‰_{V\text{-}SMOW}$	$\delta^{13}C‰_{V\text{-}PDB}$
Carbonatite	539202	calcite	12,1	−5,0
	539150a	calcite	12,3	−3,0
	539150b	calcite	12,4	−4,0
	546193	calcite	11,8	−4,3
	539202	calcite	11,9	−4,1
Melilitite	514231a	calcite	12,2	−5,2
	514239a	calcite	12,6	−5,0
	514239b	calcite	7,7	−5,0
	514231b	calcite	12,7	−6,2
Damtjernite	546054	dolomite	19,7	−2,5
	546046	dolomite	17,4	−2,3
	546054	calcite	15,6	−3,5
Limestone	Cha-1	calcite	21,2	5,0

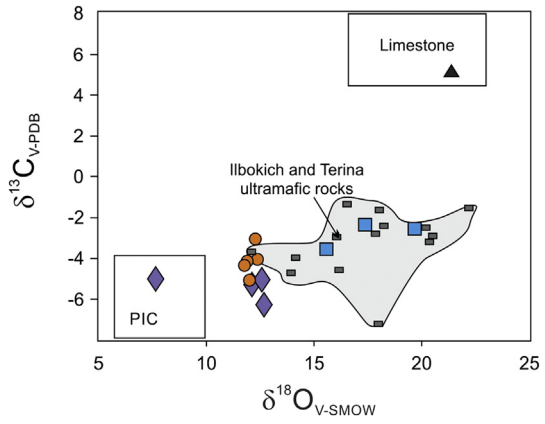

Fig. 9. $\delta^{13}C$ vs. $\delta^{18}O$ plots for carbonates from the Chuktukon rocks and country limestones (black triangle). PIC (primary igneous carbonatites) proposed by Taylor Jr and Sheppard (1986). Field for limestones from southern part of the Siberian cration is drawn from Pokrovskii et al. (2006). Field for carbonates of Terina and Ilbokich ultramafic lamprophyres is from Nosova et al. (2016). Symbols are as in Fig. 8.

Veseloe and Pogranichnoe (Doroshkevich et al., 2007a, 2007b); Wekusko Lake (Chakhmouradian et al., 2009) and Snape Lake (Agashev et al., 2008)). A number are associated with large igneous provinces (Ernst and Bell, 2010). As carbonatites from the Chuktukon are composed of nearly pure calcite, the possibility of primary origin by partial melting of carbonated peridotite can be ruled out. This is also in agreement with the mineralogical and geochemical features, such as the low concentrations of MgO, Cr and Ni, and absence of Cr-rich minerals. The formation of carbonatites as a result of the silicate-carbonate liquid immiscibility was demonstrated in early experiments (Koster van Groos and Wyllie, 1966) and has been convincingly documented in subsequent studies of volcanic rocks and melt inclusions (e.g. Guzmics et al., 2012; Mitchell and Dawson, 2012; Panina, 2005; Sekisova et al., 2015; Sharygin et al., 2012; Sokolov, 2007; Solovova and Girnis, 2012). In addition, the possibility of silicate-carbonate liquid immiscibility for the Guli massif from the primary melt of meimechite composition has been investigated by Ryabchikov and Kogarko (2016). They concluded that the sequential fractional crystallization of olivine and clinopyroxene produced residual melts which are consistent with immiscible silicate and alkali-rich carbonate liquids (Kjarsgaard, 1998). It is possible that the same mechanism has operated at Chuktukon. The alkali-rich composition of the primary carbonatite melt is supported by the fenite aureole, and the presence of Na- and K-bearing minerals (rippite, K-feldspar, tainiolite, aegirine and others) in both carbonatites and in melt and fluid inclusions (Sharygin et al., 2016b; Sharygin and Doroshkevich, 2017). Unfortunately, we did not find evidence of liquid immiscibility in melt inclusions. Textural evidence of liquid immiscibility has been described in ultramafic rocks of the Terina massif (Lapin and Pyatenko, 1992), where the rocks contain separate carbonate globules up to 2 cm in size. For this reason, to further test the silicate-carbonate liquid immiscibility mechanism for the Chuktukon rocks, partition coefficients (D) of trace element concentrations have been calculated using the experimental data of Veksler et al. (2012) and Martin et al. (2012, 2013). The calculated D carbonate/silicate Chuktukon patterns are consistent with the trace element distribution in the experimental systems (Fig. 10). A good fit of the patterns was achieved for Th, U, La, Ta, Pb, Sr and Ba. For K and Rb, the partition coefficients are low compared to experimental data. Enrichment in alkalis observed in melt inclusions (Sharygin et al., 2016b; Sharygin and Doroshkevich, 2017) and alkali-bearing minerals in carbonatites (Doroshkevich et al., 2016, Sharygin et al., 2016a, 2016b; Sharygin, 2017; Sharygin and Doroshkevich, 2017)

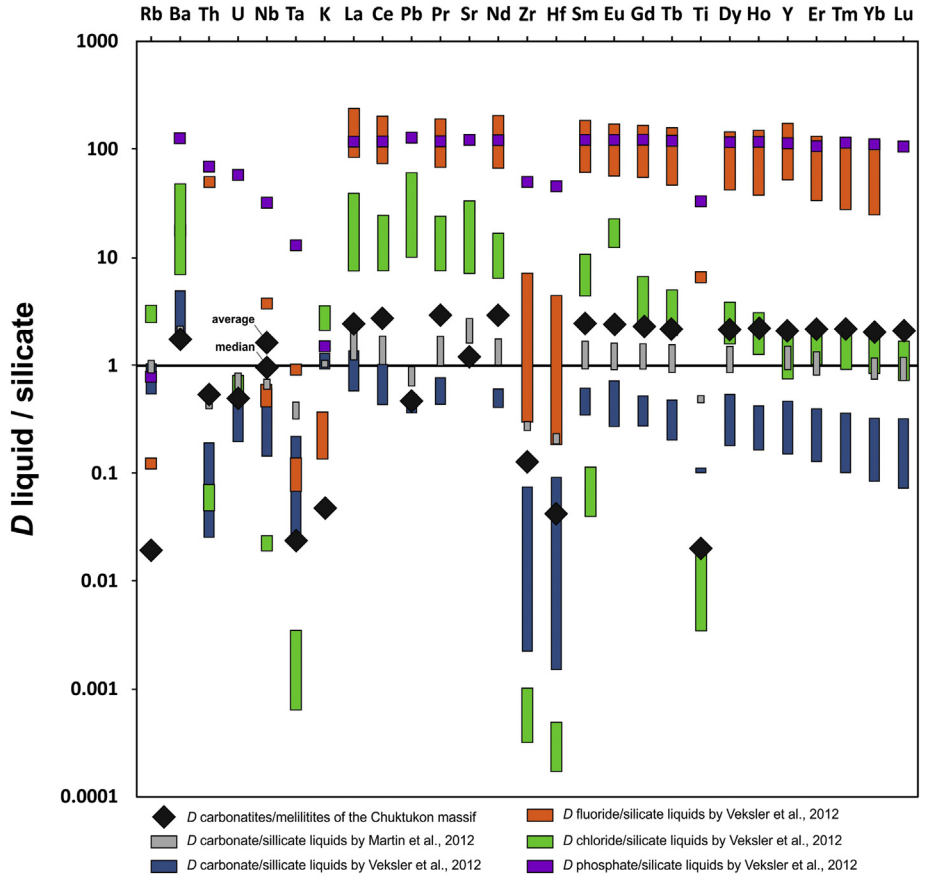

Fig. 10. Distribution coefficients (D) of trace elements between the Chuktukon carbonatites and melilitites in comparison with experimentally obtained coefficients by Martin et al. (2012, 2013) and Veksler et al. (2012).

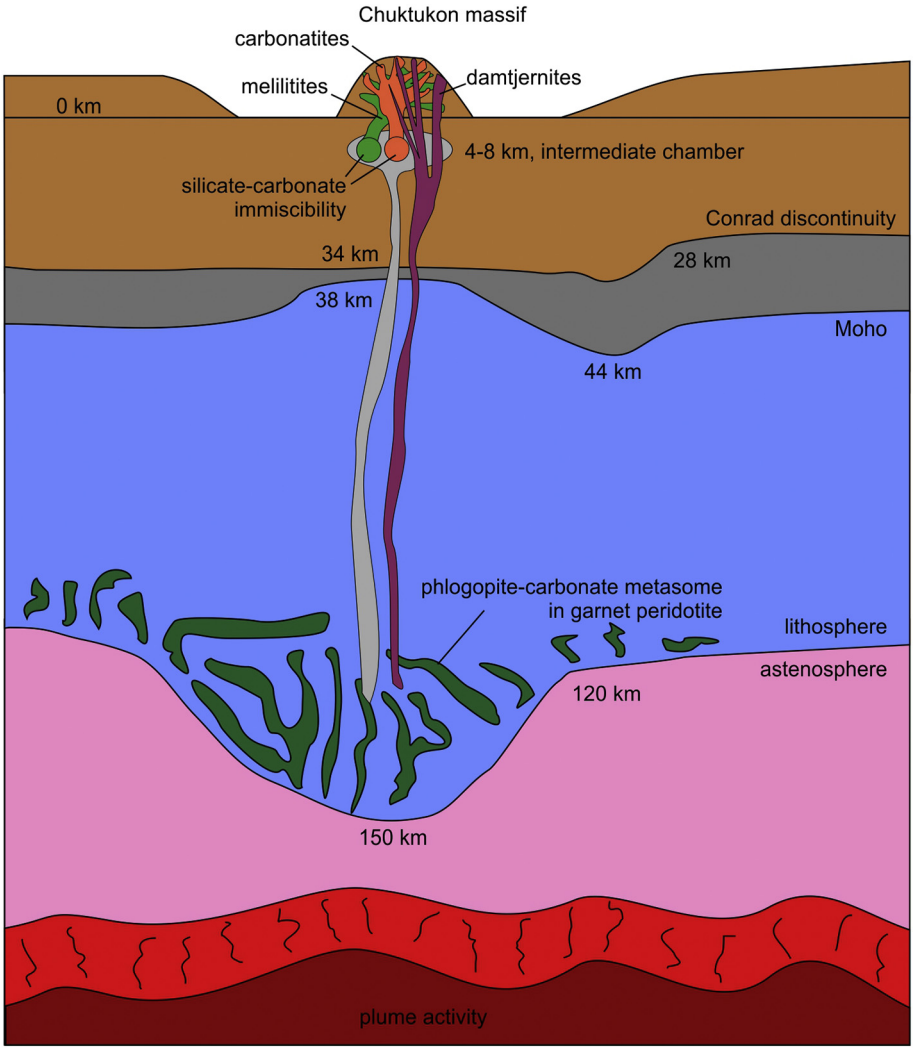

Fig. 11. Model of formation of the Chutukon massif. Locality of discontinuities are from Dashkevich (1999), locality of intermediate magmatic chamber is drawn after Kirichenko et al. (2012).

demonstrates that K was an intrinsic part of the carbonate melt. The paucity of alkali-carbonates in the rocks can be attributed to their instability and removal during hydrothermal alteration. The petrographic observations and stable isotope data are consistent with this finding. The partition coefficients for Zr, Hf and Ti in the Chuktukon rocks are lower while that of Nb is higher as compared to the experimental data on immiscible silicate and carbonate liquids (Fig. 10). The experiments have shown that HFS elements strongly concentrate in the silicate melt. For the Chuktukon, Zr—Hf, and Ti behavior is acceptable, but not for Nb. According to our geochemical data and previous investigations (Slukin, 1994; Tsikyna, 2004), the amount of Nb is highly variable (from a few to thousands ppm) in carbonatites, including weakly altered carbonatites; so if the Nb median value is used, reasonable agreement with experiments can be obtained (Fig. 10). The partition coefficients for REEs in the Chuktukon rocks are higher than their experimental values (Fig. 10). Experimental studies have demonstrated that liquid-liquid distribution coefficients for REE are close to 1, but additions of P_2O_5, F and Cl to the experimental system do reverse the REE distribution (Veksler et al., 2012) (Fig. 10). Mineralogical and geochemical data imply that the Chuktukon melts have significant amounts of halogens and P_2O_5 that play an important role in the distribution of REE. Thus, although the Chuktukon rocks are cumulates and the whole-rock compositions may differ from the compositions of the parental liquids, the trace element distribution between rocks probably can be result of liquid immiscibility. Based on the abovementioned factors, a general model for the Chuktukon evolution is presented below. The model is graphically summarized in Fig. 11.

Primary melts produced from a low degree of melting of carbonated garnet peridotite from sub-continental lithospheric mantle migrated from the source region to an intermediate magmatic chamber located at a depth of 4 km, which is confirmed by the geophysical data (Kirichenko et al., 2012).

Carbonate and silicate magmas then separated from the parental melt and subsequently transported as successive magma pulses from the subvolcanic intermediate magmatic chamber into adjacent rocks forming the sills and stocks of carbonatites and melilitites. Emplacement of these magmas was accompanied by intense hydrothermal processes that changed the stable isotope compositions. Trace element compositions of the rocks have not be changed significant during hydrothermal processes. This is clearly demonstrated by geochemical data with the comparison between Chuktukon and Terina ultramafic rocks, as well as of weakly altered and strongly altered carbonatites. The next portion of primary melt migrated from source to the surface with the formation of damtjernites, and the rapid rate of magma transport is indicated by the presence of mantle xenoliths (peridotites, eclogites) (Kirichenko et al., 2012; Lapin, 2001), the body shapes (diatremes and pipes) and abundance of pelletal lapilli in the rocks.

After emplacement all the magmatic suites, and the accompanying creation of the uplift, intense chemical weathering of the uplifted rocks and the formation of a thick weathering crust proceeded in the

Cretaceous (Chebotarev et al., 2017a) in a quiet tectonic setting with a warm humid climate (Semikhatov and Chumakov, 2004). The weathering process was accompanied by (1) element re-distribution and enrichment of the weathering crust in Zn, Th, U, Nb, Pb and REE, relative to carbonatites, melilitites and damtjernites; and (2) a change in Sr and Nd isotope composition. We interpret the modified Sr and Nd signatures as being a result of the interaction with isotopically enriched crustal-derived low-T fluids. The fluids may have mixed with an old continental crust component, acquired an extremely enriched isotope composition, and then affected previously formed alkaline rocks and carbonatites.

7.2. Relation to the Triassic Siberian LIP

The coeval Chuktukon rocks and rocks of the Maimecha-Kotuy province (meimechites, alkaline picrites, melanephelinites and rocks of the Guli alkaline ultramafic-carbonatite complex) have overlapping Sr—Nd isotopic compositions (Fig. 8), which suggests that these magma types were derived from a similar mantle source beneath the Siberian craton. Geochemical characteristics of the Chuktukon alkaline silicate rocks and the rocks of the Maimecha-Kotuy province as well as the calculated primary meimechite melt (Sobolev et al., 2009) are also similar. The Fig. 7 of the mantle-normalized trace element graphs clearly shows the correspondence for majority of elements and the similarity of the pattern shapes. Kogarko and Ryabchikov (2000), and Ryabchikov et al. (2009) suggested that the primary meimechite magmas were produced in response to mantle plume activity by a two-step process: (1) partial melting of fertile lherzolite in the asthenosphere and (2) the interaction of the melts with the lithosphere mantle material (harzburgite) during plume activity. This opinion has been supported by the discovery of metasomatized spinel lherzolite xenoliths in the Guli dunite (Panina, 2012). Sobolev et al. (2009) proposed the same model of the primary meimechite melt formation; the difference is that the metasomatic agent was silicate-carbonate melt released from recycled oceanic crust of the plume head. Alternatively, Ivanov et al. (2018) considered that the meimechite magmas could be produced by volatile fluxing of the asthenospheric mantle rather than melting caused by mantle plume activity.

However, the high-volume and short-duration Siberian flood basalts, which are temporally and spatially associated with rocks of the Chuktukon and Maimecha-Kotuy, are generally regarded as the products of mantle plume (Arndt et al., 1998; Basu et al., 1995; Burgess and Bowring, 2015; Dobretsov, 2008; Ryabchikov et al., 2009; Sobolev et al., 2009). The isotopic data of the Siberian flood basalts invariably show significant differences with respect to the Chuktukon and Maimecha-Kotuy rocks (see Fig. 8), and mostly record continental lithospheric signatures in the basalt source (e.g., Carlson et al., 2006; Fedorenko et al., 1996; Lightfoot et al., 1993; Sharma et al., 1991, 1992; Wooden et al., 1993). On the other hand, the compositions of meimechites, Guli and Chuktukon rocks lie on the starting point of a linear trend defined by the Sr—Nd isotopic compositions of the Siberian flood basalts that can indicate their genetic relationship with the Siberian mantle plume.

Carlson et al. (2006) suggested that the differing isotopic characteristics could be explained by the meimechites and the Guli rocks being located on the margin of the region of maximum flood basalt output.. This suggestion seems to be consistent with the numerical test of meimechite formation during interaction between the plume and lithosphere of the Siberian craton (Sobolev et al., 2009). Both the Chuktukon and Terina massifs from the Chadobets uplift are located at a considerable distance from the focus of the maximum magmatic activity (see Fig. 1). In the numerical plume activity model of Sobolev et al. (2009, 2011), the plume material spreads quickly along the lithosphere boundary (approximately 2000 km/Ma) eroding the lowest part of the lithosphere. It seems possible that plume material can arrive at the area beneath the projected path of emplacement of the Chadobez uplift rocks on the surface. Considering the high temperature of the plume (1600–1650 °C) and large volume of eroded lithosphere material (Sobolev et al., 2009, 2011), however, it is difficult to imagine that the primary melts for the alkaline rocks migrating considerable distances from focal zone of plume activity can preserve the initial isotopic and geochemical signatures.

Carlson et al. (2006) observed the isotopic and geochemical similarity between Siberian kimberlites of different age groups and meimechites and demonstrated that the primary magmas for the rocks were derived from a mantle source that occurred beneath Siberia prior to and after the Siberian flood-volcanic event. In our opinion, that metasomatized mantle source was heated under the influence of heat from the plume. This idea is in agreement with the light noble gas investigations of Buikin et al. (2017), who noted the absence of a plume signature in source of the Guli carbonatites. In addition, the most recently discovered occurrence of aillikite-damtjernite petrogenetic association is represented by the 392 Ma Ilbokich intrusion that is located close to the Chadobets uplift (Kargin et al., 2016). Its Sr isotopic composition (0.7033) is within the same range established for the Chuktukon and Maimecha-Kotuy rocks. At the same time, the trace element data of the Ilbokich and Chadobets olivine reveal some transformations of the lithospheric mantle due to Siberian plume activity with a simultaneous decrease in the abundance of phlogopite metasomes and increase in carbonate component (Nosova et al., 2018).

8. Conclusions

Melilitites, damtjernites and carbonatites are products from primary melts that were derived from a moderately depleted mantle. Primary melts were formed by low degree partial melting of garnet carbonated peridotite under the influence of heat from the plume. Overlapping Sr—Nd isotopic compositions of the coeval Chuktukon rocks and alkaline rocks of the Maimecha-Kotuy province suggest that these magma types were derived from a similar moderately depleted mantle source beneath the Siberian craton. Geochemical characteristics of the Chuktukon alkaline silicate rocks are similar to those of the alkaline rocks of the Maimecha-Kotuy province and of the calculated primary meimechite melt. The Chuktukon rocks were not contaminated by crustal materials during emplacement. The Chuktukon rocks have experienced hydrothermal and weathering events, which changed their isotopic and trace element characteristics and those of their mineral phases. Hydrothermal fluids altered the primary rocks, causing ^{18}O- and ^{13}C- enrichment. During weathering, interaction with crustal-derived fluids produced a change in Sr and Nd isotopic signature and caused element re-distribution and enrichment of the weathering crust in Zn, Th, U, Nb, Pb and REE, relative to the Chuktukon rocks.

Acknowledgements

Geochemical and isotopic studies of the rocks were supported by the research project of the Institute of Geology and Mineralogy SB RAS, No 0330-2016-0002. Mineralogical investigations were carried out using funds from grant of Russian Government (project no. 14.Y26.31.0012). We are grateful to the geologist A.S. Varganov and N.N. Popova from the “Krasnoyarsk geolsiemka” company for the sample collection. The authors gratefully thank Prof. Nelson Eby for the editorial comments, Prof. Richard Ernst and anonymous reviewers for the reviews and correction of the English language, which led to the significant improvement of the manuscript.

Appendix A. Supplementary data

Supplementary data to this article can be found online at https://doi.org/10.1016/j.lithos.2019.03.006.

References

Agashev, A.M., Pokhilenko, N.P., Takazawa, E., McDonald, J.A., Vavilov, M.A., Watanabe, T., Sobolev, N.V., 2008. Primary melting sequence of a deep (>250 km) lithospheric mantle as recorded in the geochemistry of kimberlite–carbonatite assemblages, Snap Lake dyke system, Canada. Chemical Geology 255, 317–328. https://doi.org/10.1016/j.chemgeo.2008.07.003.

Arndt, N., Chauvel, C., Czamanske, G., Fedorenko, V., 1998. Two mantle sources, two plumbing systems: tholeiitic and alkaline magmatism of the Maymecha River basin, Siberian flood volcanic province. Contributions to Mineralogy and Petrology 133, 297–313. https://doi.org/10.1007/s004100050453.

Ballhaus, C.B., Berry, R.F., Green, D.H., 1991. High pressure experimental calibration of the olivine-orthopyroxene-spinel oxygen barometer—implications for redox conditions in the upper mantle. Contributions to Mineralogy and Petrology 107, 27–40.

Basu, A.R., Poreda, R.J., Renne, P.R., Telchmann, F., Vasiliev, Y.R., Sobolev, N.V., Turrin, B.D., 1995. High-^{3}He plume origin and temporal–spatial evolution of the Siberian flood basalts. Science 269 (5225), 825–882. https://doi.org/10.1126/science.269.5225.822.

Bell, K., Rukhlov, A.S., 2004. Carbonatites from the Kola Alkaline Province: origin, evolution and source characteristics. In: Wall, F., Zaitsev, A.N. (Eds.), Phoscorites and Carbonatites From Mantle to Mine: The Key Example of the Kola Alkaline Province. vol. 10. Mineralogical Society Series, London, pp. 433–468.

Bouvier, A., Vervoort, J.D., Patchett, P.J., 2008. The Lu–Hf and Sm–Nd isotopic composition of CHUR: Constraints from unequilibrated chondrites and implications for the bulk composition of terrestrial planets. Earth and Planetary Science Letters 273 (1–2), 48–57. https://doi.org/10.1016/j.epsl.2008.06.010.

Buikin, A.I., Kogarko, L.N., Hopp, J., Trieloff, M., 2017. Light noble gas data in Guli massif carbonatites reveal the subcontinental lithospheric mantle as primary fluid source. Geochemistry International 55 (5), 457–464. https://doi.org/10.1134/S0016702917050056.

Burgess, S.D., Bowring, S.A., 2015. High-precision geochronology confirms voluminous magmatism before, during, and after Earth's most severe extinction. Science Advances 1 (7), e1500470. https://doi.org/10.1126/sciadv.1500470.

Carlson, R.W., Czamanske, G., Fedorenko, V., Ilupin, I., 2006. A comparison of Siberian meimechites and kimberlites: implications for the source of high-Mg alkalic magmas and flood basalts. Geochemistry, Geophysics, Geosystems 7 (11). https://doi.org/10.1029/2006GC001342.

Chakhmouradian, A.R., Böhm, C.O., Demèny, A., Reguir, E.P., Hegner, E., Creaser, R.A., Halden, N.M., Yang, P., 2009. "Kimberlite" from Wekusko Lake, Manitoba: actually a diamond-indicator-bearing dolomite carbonatite. Lithos 112S, 347–357.

Chebotarev, D.A., Doroshkevich, A.G., Sharygin, V.V., Yudin, D.S., Ponomarchuk, A.V., Sergeev, S.A., 2017a. Geochronology of the Chuktukon carbonatite massif, Chadobets uplift (Krasnoyarsk Territory). Russian Geology and Geophysics 58, 1222–1231. https://doi.org/10.1016/j.rgg.2017.02.003.

Chebotarev, D.A., Doroshkevich, A.G., Klemd, R., Karmanov, N.S., 2017b. Evolution of Nb-mineralization in the Chuktukon carbonatite massif, Chadobets upland (Krasnoyarsk Territory, Russia). Periodico di Mineralogia 86, 99–118. https://doi.org/10.2451/2017PM733.

Dalrymple, G.B., Czamanske, G.K., Fedorenko, V.A., Simonov, O.N., Lanphere, M.A., Likhachev, A.P., 1995. A reconnaissance $^{40}Ar/^{39}Ar$ geochronologic study of ore-bearing and related rocks, Siberian Russia. Geochimica et Cosmochimica Acta 59 (10), 2071–2083. https://doi.org/10.1016/0016-7037(95)00127-1.

Dalton, J.A., Presnall, D.C., 1998. The continuum of primary carbonatitic-kimberlitic melt compositions in equilibrium with lherzolite: Data from the system CaO-MgO-Al_2O_3–SiO_2–CO_2 at 6 GPa. Journal of Petrology 39, 1953–1964. https://doi.org/10.1093/petroj/39.11-12.1953.

Dasgupta, R., Hirschmann, M.M., McDonough, W.F., Spiegelman, M., Withers, A.C., 2009. Trace element partitioning between garnet lherzolite and carbonatite at 6.6 and 8.6 GPa with applications to the geochemistry of the mantle and of mantle-derived melts. Chemical Geology 262, 57–77. https://doi.org/10.1016/j.chemgeo.2009.02.004.

Dashkevich, N.N., 1999. Regional prediction of kimberlite magmatism in the southwestern Siberian Platform. Geologiya i poleznye iskopaemye Krasnoyarskogo kraya (Geology and Mineral Resources of Krasnoyarsk District) in Russian 31–42.

Deines, P., 1989. Stable isotope varition in carbonatites. In: Bell, K. (Ed.), Carbonatites: Genesis and Evolution. Hyman, London, pp. 301–359.

Demény, A., Sitnikova, M.A., Karchevsky, P.I., 2004. Stable C and O isotope compositions of carbonatite complexes of the Kola Alkaline Province: phoscorite–carbonatite relationships and source compositions. In: Wall, F., Zaitsev, A.N. (Eds.), Phoscorites and Carbonatites From Mantle to Mine: the Key Example of the Kola Alkaline Province. vol. 10. Mineralogical Society Series, London, pp. 407–431.

Dobretsov, N.L., 2008. Geological implications of the thermochemical plume model. Russian Geology and Geophysics 49 (7), 441–454. https://doi.org/10.1016/j.rgg.2008.06.002.

Doroshkevich, A.G., Wall, F., Ripp, G.S., 2007a. Magmatic graphite in dolomite carbonatite at Pogranichnoe, North Transbaikalia, Russia. Contributions to Mineralogy and Petrology 153, 339–353.

Doroshkevich, A.G., Wall, F., Ripp, G.S., 2007b. Calcite-bearing dolomite carbonatite dykes from Veseloe, North Transbaikalia, Russia and possible Cr-rich mantle xenoliths. Mineralogy and Petrology 90, 19–49.

Doroshkevich, A.G., Ripp, G.S., Viladkar, S., 2010. Newania carbonatites, Western India: example of mantle derived magnesium carbonatites. Mineralogy and Petrology 98, 283–295.

Doroshkevich, A.G., Sharygin, V.V., Seryotkin, Y.V., Karmanov, N.S., Belogub, E.V., Moroz, T.N., Nigmatulina, E.N., Eliseev, A.P., Vedenyapin, V.N., Kupriyanov, I.N., 2016. Rippite, IMA 2016-025. CNMNC newsletter no. 32, August 2016, page 919. Mineralogical Magazine 80 (6), 915–922.

Downes, H., Kostoula, T., Jones, A.P., Beard, A.D., Thirlwall, M.F., Bodinier, J.-L., 2002. Geochemistry and Sr–Nd isotopic compositions of mantle xenoliths from the Monte Vulture carbonatite–melilitite volcano, central southern Italy. Contributions to Mineralogy and Petrology 144 (1), 78–92. https://doi.org/10.1007/s00410-002-0383-4.

Downes, H., Balaganskaya, E., Beard, A.D., Liferovich, R., Demaiffe, D., 2005. Petro-genetic processes in the ultramafic, alkaline and carbonatitic magmatism in the Kola Alkaline Province: a review. Lithos 85, 48–75. https://doi.org/10.1016/j.lithos.2005.03.020.

Ernst, R.E., Bell, K., 2010. Large igneous provinces (LIPs) and carbonatites. Mineralogy and Petrology 98, 55–76. https://doi.org/10.1007/s00710-009-0074-1.

Ernst, R.E., Davies, D.R., Jowitt, S.M., Campbell, I.H., 2018. When do mantle plumes destroy diamonds? Earth and Planetary Science Letters. 502, 244–252. https://doi.org/10.1016/j.epsl.2018.08.058.

Fedorenko, V.A., Lightfoot, P.C., Naldrett, A.J., Czamanske, G., Hawkesworth, C., Wooden, J., Ebel, D., 1996. Petrogenesis of the Siberian flood-basalt sequence at Noril'sk, north Central Siberia. International Geology Review 38, 99–135. https://doi.org/10.1080/00206819709465327.

Fedorenko, V., Czamanske, G., Zenko, T., Budahn, J., Siems, D., 2000. Field and Geochemical Studies of the Melilite-Bearing Arydzhangsky Suite, and an overall Perspective on the Siberian Alkaline–Ultramafic Flood-Volcanic Rocks. International Geology Review 42, 769–804. https://doi.org/10.1080/00206810009465111.

Foley, S.F., Yaxley, G.M., Rosenthal, A., Buhre, S., Kiseeva, E.S., Rapp, R.P., Jacob, D.E., 2009. The composition of near-solidus melts of peridotite in the presence of CO_2 and H_2O between 40 and 60 kbar. Lithos 112, 274–283. https://doi.org/10.1016/j.lithos.2009.03.020.

Ghobadi, M., Gerdes, A., Kogarko, L., Hoefer, H., Brey, G., 2018. In situ LA-ICPMS Isotopic and Geochronological Studies on Carbonatites and Phoscorites from the Guli Massif, Maymecha-Kotuy, Polar Siberia. Geochemistry International 56 (8), 766–783. https://doi.org/10.1134/S0016702918080049.

Goldstein, S.J., Jacobsen, S.B., 1988. Nd and Sr isotopic systematics of river water suspended material implications for crystal evolution. Earth and Planetary Science Letters 87 (3), 249–265. https://doi.org/10.1016/0012-821X(88)90013-1.

Gudfinnsson, G.H., Presnall, D.C., 2005. Continuous gradations among primary carbonatitic, kimberlitic, melilititic, basaltic and komatiitic melts in equilibrium with garnet lherzolite at 3–8 GPa. Journal of Petrology 46, 1645–1659. https://doi.org/10.1093/petrology/egi029.

Guzmics, T., Mitchel, R.H., Szabo, C., Berkesi, M., Milke, R., Ratter, K., 2012. Liquid immiscibility between silicate, carbonate and sulfide melts in melt inclusions hosted in co-precipitated minerals from Kerimasi volcano (Tanzania): evolution of carbonated nephelinitic magma. Contributions to Mineralogy and Petrology 164, 101–122. https://doi.org/10.1007/s00410-012-0728-6.

Harmer, R.E., 1999. The petrogenetic association of carbonatite and alkaline magmatism: constraints from the Spitskop complex, South Africa. Journal of Petrology 40, 525–548.

Harmer, R.E., Gittins, J., 1998. The case for primary, mantle-derived carbonatite magma. Journal of Petrology 39, 1895–1903.

Howarth, G.H., Barry, P.H., Pernet-Fisher, J.F., Baziotis, I.P., Pokhilenko, N.P., Pokhilenko, L.N., Bodnar, R.J., Taylor, L.A., Agashev, A.M., 2014. Superplume metasomatism: evidence from Siberian mantle xenoliths. Lithos 184–187, 209–224. https://doi.org/10.1016/j.lithos.2013.09.006.

Ivanov, A.V., He, H., Yan, L., Ryabov, V.V., Shevko, A.Y., Palesskii, S.V., Nikolaeva, I.V., 2013. Siberian Traps large igneous province: evidence for two food basalt pulses around the Permo–Triassic boundary and in the Middle Triassic, and contemporaneous granitic magmatism. Earth-Science Reviews 122, 58–76. https://doi.org/10.1016/j.earscirev.2013.04.001.

Ivanov, A.V., Mukasa, S.B., Kamenetsky, V.S., Ackerson, M., Demonterova, E.I., Pokrovsky, B.G., Vladykin, N.V., Kolesnichenko, M.V., Litasov, K.D., Zedgenizov, D.A., 2018. Volatile concentrations in olivine-hosted melt inclusions from meimechite and melanephelinite lavas of the Siberian Traps Large Igneous Province: evidence for flux-related high-Ti, high-Mg magmatism. Chemical Geology 483, 442–462.

Kargin, A.V., Nosova, A.A., Chugaev, A.V., Sazonova, L.V., Dokuchaev, A.Y., Smirnova, M.D., Postnikov, A.V., Postnikova, O.V., Popova, L.P., Poshibaev, V.V., 2016. Devonian ultramafic lamprophyre in the Irkineeva–Chadobets trough in the southwest of the Siberian platform: age, composition, and implications for diamond potential prediction. Geology and Ore Deposits 58 (5), 383–403. https://doi.org/10.1134/S1075701516050068.

Kirichenko, T., Zuev, K., Perfilova, O.Yu., Sosnovskaya, O., Smokotina, I., Markovich, L.A., Borodin, Mironyuk E., 2012. State Geological Map of Russian Federation, Scale 1: 1000000 (Third Generation). Ser. Angaro-Eniseysk. Sheet O-47 Bratsk. Explanatory Note. Cartografic Factory of VSEGEI, St. Petersburg, pp. 163–179 (In Russian).

Kjarsgaard, B.A., 1998. Phase relations of a carbonated high-CaO nephelinite at 0.2 and 0.5 GPa. Journal of Petrology 39, 2061–2075. https://doi.org/10.1093/petroj/39.11-12.2061.

Klemme, S., Vanderlaan, S.R., Foley, S.F., Gunther, D., 1995. Experimentally determined trace and minor element partitioning between clinopyroxene and carbonatite melt under upper-mantle conditions. Earth and Planetary Science Letters 133, 439–448. https://doi.org/10.1016/0012-821X(95)00098-W.

Kogarko, L.N., Ryabchikov, I.D., 2000. Geochemical evidence for meimechite magma generation in the subcontinental lithosphere of Polar Siberia. Journal of Asian Earth Sciences 18, 195–203. https://doi.org/10.1016/S1367-9120(99)00041-3.

Kogarko, L.N., Zartman, R.E., 2011. New data on the age of the Guli intrusion and implications for the relationships between alkaline magmatism in the Maymecha–Kotuy province and the Siberian Superplume: U–Th–Pb isotopic systematics. Geochemistry International 49 (5), 439–448. https://doi.org/10.1134/S0016702911050065.

Kogarko, L.N., Kurat, G., Ntaflos, T., 2007. Henrymeyerite in the metasomatized upper mantle of eastern Antarctica. The Canadian Mineralogist 45 (3), 497–501. https://doi.org/10.2113/gscanmin.45.3.497.

Kogarko, L.N., Ryabchikov, I.D., Kuzmin, D.V., 2012. High-Ba mica in olivinites of the Guli massif (Maymecha–Kotuy province, Siberia). Russian Geology and Geophysics 53 (11), 1209–1215. https://doi.org/10.1016/j.rgg.2012.09.007.

Koster van Groos, A.F., Wyllie, P.J., 1966. Experimental Data bearing on the Role of Liquid Immiscibility in the Genesis of Carbonatites. Nature 199, 801–802. https://doi.org/10.1038/199801a0.

Lapin, A.V., 1997. Structure, formation conditions and ore-bearing of the main types of REE in the carvonatite weathering crusts. Otechestvennaya Geologiya 11, 15–22 (In Russian).

Lapin, A.V., 2001. About kimberlites of the Chadobets upland in connection with a problem of the formational-metallogeny analysis of the platform alkaline ultrabasic magmatic rocks. Otechestvennaya Geologiya 4, 30–35 (In Russian).

Lapin, A.V., Lisitzyn, D.V., 2004. About mineralogical typomorphism of alkaline ultrabasic magmatic rocks of Chadobets upland. Otechestvennaya Geologiya 683, 93 (In Russian).

Lapin, A.V., Pyatenko, I.K., 1992. Chadobets complex of ultrabasic alkaline rocks and carbonatites: new data about composition and condition of formation. Doklady Earth Sciences 6, 88–101 (In Russian).

Letnikova, E.F., Izokh, A.E., Nikolenko, E.I., Pokhilenko, N.P., Shelestov, V.O., Geng, Hilen, Lobanov, S.S., 2014. Late Triassic high-potassium trachitic volcanism of the northeast of the Siberian platform: evidence in the sedimentary record. Doklady Earth Sciences 459 (1), 1344–1347. https://doi.org/10.1134/S1028334X14110221.

Lightfoot, P.C., Hawkesworth, C.J., Hergt, J., Naldrett, A.J., Gorbachev, N.S., Fedorenko, V.A., Doherty, W., 1993. Remobilization of the continental lithosphere by a mantle plume: major-, trace-element, and Sr-, Nd- and Pb-isotopic evidence from picritic and tholeiitic lavas of the Noril'sk district, Siberia. Contributions to Mineralogy and Petrology 114, 171–188. https://doi.org/10.1007/BF00307754.

Lomayev, V.G., Serdyuk, S.S., 2011. The Chuktukon Nb-TR deposit - the priority object for modernization of the Russian rare-earth industry. Journal of Siberian Federal University 4, 132–154.

Malich, K.N., Khiller, V.V., Badanina, I.Yu., Belousova, E.A., 2015. Results of dating of thorianite and baddeleyite from carbonatites of the Guli massif. Russian Doklady Earth Sciences 464 (2), 1029–1032. https://doi.org/10.1134/S1028334X15100050.

Martin, L.H.J., Schmidt, M.W., Hannes, B., Mattsson, H.B., Ulmer, P., Hametner, K., Günther, D., 2012. Element partitioning between immiscible carbonatite–kamafugite melts with application to the Italian ultrapotassic suite. Chemical Geology 320-321, 96–112. https://doi.org/10.1016/j.chemgeo.2012.05.019.

Martin, L.H.J., Schmidt, M.W., Mattson, H.B., Guenther, D., 2013. Element partitioning between immiscible carbonatite and silicate melts from dry and H_2O-bearing systems at 1-3 GPa. Journal of Petrology 54, 2301–2338. https://doi.org/10.1093/petrology/egt048.

Mitchell, R.H., 1995. Kimberlite, Orangeites and Related Rocks. Plenum Press, New York.

Mitchell, R.H., Dawson, J.B., 2012. Carbonate-silicate immiscibility and extremely peralkaline silicate glasses from Nasira cone and recent eruptions at Oldoinyo Lengai Volcano, Tanzania. Lithos 152, 40–46. https://doi.org/10.1016/j.lithos.2012.01.006.

Mourtada, S., Le Bas, M.J., Pin, C., 1997. Petrogenesis of Mg-carbonatites from Tamazert in the Moroccan High Atlas. CR Academic Sciences II A 325, 559–564.

Nosova, A.A., Dubinina, E.O., Kargin, A.V., Yutkina, E.V., 2016. Isotopic ($\delta_{13}C$-$\delta^{18}O$) systematics of carbonates from alkaline ultrabasic rocks of the East-European and Siberian cratons. Abstract Volume of XXI Symposium of the Stable Isotopes Geochemistry, Moscow, Russia, 15–17 November, pp. 112–115.

Nosova, A.A., Sazonova, L.V., Kargin, A.V., Smirnova, M.D., Lapin, A.V., Shcherbakov, V.D., 2018. Olivine in ultramafic lamprophyres: chemistry, crystallisation, and melt sources of Siberian Pre- and post-trap aillikites. Contributions to Mineralogy and Petrology 173, 55. https://doi.org/10.1007/s00410-018-1480-3.

Panina, L.I., 2005. Multiphase carbonate–salt immiscibility in carbonate melts: data on melt inclusions from the Krestovskiy massif minerals (Polar Siberia). Contributions to Mineralogy and Petrology 150, 19–36. https://doi.org/10.1007/s00410-005-0001-3.

Panina, L.I., 2012. Microxenoliths of metosomatized spinel lherzolites in dunites from the Guli Pluton. Abstract Volume of XXIX International Conference «Ore Potential of Alkaline, Kimberlite and Carbonatite Magmatism», Sudak-Moscow, Russia, 14-22 September , pp. 110–111. http://alkaline.web.ru/2012/abstracts/Panina.htm.

Pokrovskii, B.G., Melezhik, V.A., Bujakaite, M.I., 2006. Carbon, oxygen, strontium, and sulfur isotopic compositions in late Precambrian rocks of the Patom complex, Central Siberia: communication 1. Results, isotope stratigraphy, and dating problems. Lithology and Mineral Resources 41 (5), 450–474.

Rudnick, R.L., Gao, S., 2003. Composition of the continental crust. In: Rudnick, R.L. (Ed.), Treatise on Geochemistry. Elsevier, Amsterdam, pp. 1–64 https://doi.org/10.1016/B0-08-043751-6/03016-4.

Ryabchikov, I.D., Kogarko, L.N., 2016. Deep differentiation of alkali ultramafic magmas: formation of carbonatite melts. Geochemistry International 54 (9), 739–747. https://doi.org/10.1134/S001670291609007X.

Ryabchikov, I.D., Kogarko, L.N., Solovova, I.P., 2009. Physicochemical conditions of magma formation at the base of the Siberian plume: insight from the investigation of melt inclusions in the meymechites and alkali picrites of the Maimecha—Kotui Province. Petrology 17, 287–299. https://doi.org/10.1134/S0869591109030059.

Santos, R.V., Clayton, R.N., 1995. Variations of oxygen and carbon isotopes in carbonatites: a study of Brazilian alkaline complexes. Geochimica et Cosmochimica Acta 59, 1339–1352.

Sekisova, V.S., Sharygin, V.V., Zaitsev, A.N., Strekopytov, S., 2015. Liquid immiscibility during crystallization of forsterite–phlogopite ijolites at Oldoinyo Lengai Volcano, Tanzania: study of melt inclusions. Russian Geology and Geophysics 56, 1717–1737.

Semikhatov, M.A., Chumakov, N.M., 2004. Climate in the Epochs of Major Biosphere Transformations. Nauka, Moscow (in Russian).

Sharma, M., Basu, A.R., Nesterenko, G.V., 1991. Nd-Sr isotopes, petrochemistry, and origin of the Siberian flood basalts, USSR. Geochimica et Cosmochimica Acta 53, 1183–1192. https://doi.org/10.1016/0016-7037(91)90177-7.

Sharma, M., Basu, A.R., Nesterenko, G.V., 1992. Temporal Sr-, Nd-, and Pb-isotopic variations in the Siberian flood basalts: implications for the plume-source characteristics. Earth and Planetary Science Letters 113, 365–381. https://doi.org/10.1016/0012-821X(92)90139-M.

Sharygin, V.V., 2017. Tainiolite from Chuktukon Carbonatite Massif, Chadobets Upland, Russia. Abstract Volume of XXXIV International Conference "Magmatism of the Earth and Related Strategic Metal Deposits", Miass, 4–9 August 2017, pp. 242–244.

Sharygin, V.V., Doroshkevich, A.G., 2017. Multiphase inclusions in zircons from Chuktukon carbonatite massif, Chadobets upland, Russia. Abstract Volume of XXXIV International Conference "Magmatism of the Earth and Related Strategic Metal Deposits", Miass, 4–9 August, pp. 244–247.

Sharygin, V.V., Kamenetsky, V.S., Zaitsev, A.N., Kamenetsky, M.B., 2012. Silicate-natrocarbonatite liquid immiscibility in 1917 eruption combeite-wollastonite nephelinite, Oldoinyo Lengai Volcano, Tanzania: Melt inclusion study. Lithos 152, 23–39. https://doi.org/10.1016/j.lithos.2012.01.021.

Sharygin, V.V., Doroshkevich, A.G., Seryotkin, Y.V., Karmanov, N.S., Belogub, E.V., Moroz, T.N., 2016a. A new K-Nb cyclosilicate $K_2(Nb,Ti)_2(Si_4O_{12})O(O,F)$ from Chuktukon carbonatite massif, Chadobets upland, Russia. Abstract Volume of Second European Mineralogical Conference, Rimini, Italy, 11–15 September, p. 421.

Sharygin, V.V., Doroshkevich, A.G., Chebotarev, D.A., 2016b. Na-Sr-Ba-REE-carbonates and phosphates in minerals of Chuktukon massif carbonatites, Chadobets upland, Krasnoyarsk territory. Abstract Volume of XVII Russian Fluid Inclusion Conference, Ulan-Ude, Russia, pp. 180–182.

Slukin, A.D., 1994. Bauxite deposits with unusually high concentrations of REE, Nb, Ti, and Th, Chadobets uplift, Siberian platform. International Geology Review 36 (2), 179–193. https://doi.org/10.1080/00206819409465454.

Sobolev, A.V., Sobolev, S.V., Kuzmin, D.V., 2009. Siberian meimechites: origin and relation to flood basalts and kimberlites. Russian Geology and Geophysics 50, 999–1033. https://doi.org/10.1016/j.rgg.2009.11.002.

Sobolev, S.V., Sobolev, A.V., Kuzmin, D.V., Krivolutskaya, N.A., Petrunin, A.G., Arndt, N.T., Radko, V.A., Vasiliev, Y.R., 2011. Nature 477, 312–316. https://doi.org/10.1038/nature10385.

Sokolov, S.V., 2007. Phase composition of melt inclusions in monticellite and niocalite from carbonatites of the Oka complex (Quebec, Canada): confirmation of silicate–carbonate liquid immiscibility. Abstracts of ECROFI-XIX. University of Bern, Switzerland, p. 202 (17-20 July).

Solovova, I.P., Girnis, A.V., 2012. Silicate-carbonate liquid immiscibility and crystallization of carbonate and K-rich basaltic magma: insights from melt and fluid inclusions. Mineralogical Magazine 76, 411–439. https://doi.org/10.1180/minmag.2012.076.2.09.

Staroseltsev, V.S., 2009. Identifying paleorifts as promising tectonic elements for active oil and gas generation. Russian Geology and Geophysics 50 (4), 358–364.

Sun, S.-S., McDonough, W.F., 1989. Chemical and isotopic systematics of oceanic basalts: implications for mantle composition and processes. Geological Society of London, Special Publications 42, 313–345. https://doi.org/10.1144/GSL.SP.1989.042.01.19.

Sun, J., Liu, C., Tappe, S., Kostrovitsky, S.I., Wu, F.-Y., Yakovlev, D., Yang, Y.-H., Yang, J.-H., 2014. Repeated kimberlite magmatism beneath Yakutia and its relationship to Siberian flood volcanism: Insights from in situ U–Pb and Sr–Nd perovskite isotope analysis. Earth and Planetary Science Letters 404, 283–295. https://doi.org/10.1016/j.epsl.2014.07.039.

Sweeney, R.J., Prozesky, V., Przybylowicz, W., 1995. Selected trace and minor element partitioning between peridotite minerals and carbonatite melts at 18–46 kbar pressure. Geochimica et Cosmochimica Acta 59, 3671–3683. https://doi.org/10.1016/0016-7037(95)00270-A.

Tappe, S., Foley, S.F., Jenner, G.A., Kjarsgaard, B.A., 2005. Integrating ultramafic lamprophyres into the IUGS classification of igneous rocks: rational and implications. Journal of Petrology 46, 1893–1900.

Tappe, S., Romer, R.L., Stracke, A., Steenfelt, A., Smart, K.A., Muehlenbachs, K., Torsvik, T.H., 2017. Sources and mobility of carbonate melts beneath cratons, with implications for deep carbon cycling, metasomatism and rift initiation. Earth and Planetary Science Letters 466, 152–167. https://doi.org/10.1016/j.epsl.2017.03.011.

Taylor Jr., H.P., Sheppard, S.M.F., 1986. Stable isotopes in high temperature geological processes. In: Valley, J.W., Taylor Jr., H.P., O'Neil, J.R. (Eds.), Stable Isotopes in High Temperature Geological Processes. Rev. Mineral vol. 16, pp. 227–269.

Tsikyna, S.V., 2004. The Nb-REE Chuktukon Deposit. Modelling, Ore Typification and Assessment of Prospects. the Krasnoyarsk Research Institute of Geology and Mineral Resources (Ph.D. thesis, In Russian).

Vasilyev, Yu.P., Gora, M.P., Kuzmin, D.V., 2017. Meimechite-Foidite Volcanism of Polar Siberia. Izdatelstvo SB RAS, Novosibirsk (In Russian).

Vasyukova, E.A., 2017. Petrology and Fluid Regime of Formation of Chuiskii Lamproites (South-East Altay and North-West Mongolia). Izdatelstvo SB RAS, Novosibirsk (In Russian).

Veksler, I.V., Dorfman, A.M., Dulski, P., Kamenetsky, V.S., Danyushevsky, L.V., Jeffries, T., Dingwell, D.B., 2012. Partitioning of elements between silicate melt and immiscible fluoride, chloride, carbonate, phosphate and sulfate melts with implications to the origin of natrocarbonatite. Geochimica et Cosmochimica Acta 79, 20–40. https://doi.org/10.1016/j.gca.2011.11.035.

Vrublevskii, V.V., Voitenko, N.N., Romanov, A.P., Polyakov, G.V., Izokh, A.E., Gertner, I.F., Krupchatnikov, V.I., 2005. Magma sources of Triassic lamproites of Gornyi Altai and Taimyr: Sr and Nd isotope evidence for plume–lithosphere interaction. Doklady Earth Sciences 405a (9), 1365–1367.

Walter, M.J., Bulanova, G.P., Armstrong, L.S., Keshav, S., Blundy, J.D., Gudfinnsson, G., Lord, O.T., Lennie, A.R., Clark, S.M., Smith, C.B., Gobbo, L., 2008. Primary carbonatite melt from deeply subducted oceanic crust. Nature 454, 622–626. https://doi.org/10.1038/nature07132.

Whitney, D.L., Evans, B.W., 2010. Abbreviations for names of rock-forming minerals. American Minerologist 95, 185–187.

Wooden, J.L., Czamanske, G.K., Fedorenko, V.A., Arndt, N.T., Chauvel, C., Bouse, R.M., King, B.-S.W., Knight, R.J., Siems, D.F., 1993. Isotopic and trace-element constraints on mantle and crustal contributions to Siberian continental flood basalts, Noril'sk area, Siberia. Geochimica et Cosmochimica Acta 57, 3677–3704. https://doi.org/10.1016/0016-7037(93)90149-Q.

Zaitsev, A.P., Smelov, A.P., 2010. Isotopic Geochronology of the Rocks of the Yakutian Kimberlite Province. DPMGI SB RAS, Yakutsk (In Russian).